

Dilation of subglacial sediment governs incipient surge motion in glaciers with deformable beds

Brent M. Minchew¹ and Colin R. Meyer²

¹Department of Earth, Atmospheric and Planetary Sciences, Massachusetts Institute of Technology, Cambridge, MA, USA

²Thayer School of Engineering, Dartmouth College, Hanover, NH, USA

Corresponding author: B. M. Minchew, minchew@mit.edu

Abstract

Glacier surges are quasi-periodic episodes of rapid ice flow that arise from increases in slip-rate at the ice-bed interface. The mechanisms that trigger and sustain surges are not well-understood. Here, we develop a new model of incipient surge motion for glaciers underlain by sediments to explore how surges may arise from slip instabilities within this thin layer of saturated, deforming subglacial till. Our model represents the evolution of internal friction, porosity, and pore water pressure within the sediments as functions of the rate and history of shearing. Changes in pore water pressure govern incipient surge motion, with less-permeable till facilitating surging because dilation-driven reductions in pore-water pressure slow the rate at which till tends toward a new steady state, thereby allowing time for the glacier to thin dynamically. The reduction of overburden pressure at the bed caused by dynamic thinning of the glacier sustains surge acceleration in our model. The need for changes in both the hydromechanical properties of the till and thickness of the glacier creates restrictive conditions for surge motion that are consistent with the rarity of surge-type glaciers and their geographic clustering.

Subjects: glaciology, geophysics, mathematical modeling

Keywords: glacier surges, glacier dynamics, granular mechanics

1 Introduction

Surges are enigmatic characteristics of glacier flow. Broadly speaking, glacier surges are sub-annual to multi-annual periods of relatively rapid flow that occur quasi-periodically, with quiescent periods between surges ranging from several years to centuries (Meier and Post, 1969; Raymond, 1987). Flow velocities during a surge can reach 5–100 times typical quiescent-phase velocities because of commensurate increases in the rate of slip at the ice-bed interface, hereafter called basal slip rate. Accelerated basal slip rates are facilitated by changes in the mechanical, thermal, and hydrological properties of the bed, which may work independently or in concert to initiate, sustain, and arrest glacier surges (Raymond, 1987; Kamb, 1987; Murray et al., 2000; Fowler et al., 2001; Murray et al., 2003; Flowers et al., 2011; Meyer et al., 2016; Flowers et al., 2016; Benn et al., 2019).

Surges are known to occur in only about 1% of glaciers worldwide (Jiskoot et al., 1998; Sevestre and Benn, 2015). Known surge-type glaciers are clustered in a handful of globally dispersed geographic regions, share comparable geological factors, but inhabit a variety of climates (Meier and Post, 1969; Sevestre and Benn, 2015; Jiskoot et al., 2000). A common feature identified in surge-type glaciers is the presence of mechanically weak beds consisting of thick layers of water-saturated, deformable sediment and erodible sedimentary or volcanic rock (Truffer et al., 2000; Björnsson et al., 2003; Harrison and Post, 2003; Woodward et al., 2003). This commonality suggests that the mechanics of deformable glacier beds play an important role in initiating and sustaining glacier surges. However, the fact that not every glacier underlain

37 by sediments surges indicates that the existence of a deformable bed is not a sufficient condition for surging
38 (Harrison and Post, 2003). Despite the prevalence of till, many existing surge models ignore till mechanics
39 and consider only rigid, impermeable beds, often with a focus on the hydrological and thermal states (Benn
40 et al., 2019; Fowler, 2011).

41 The prevailing model of glacier surges posits that incipient surge motion arises from a switch in the
42 subglacial hydrological system from a relatively efficient channelized system to an inefficient distributed, or
43 linked-cavity, system (Kamb, 1987; Benn et al., 2019; Kamb et al., 1985). Throughout the surge phase, the
44 basal hydrological system likely remains relatively inefficient, facilitating rapid basal slip due to lubrication
45 from high basal water pressures, until reestablishment of an efficient channelized system reduces basal water
46 pressure and terminates the surge (Kamb et al., 1985; Bjornsson, 1998; Pritchard et al., 2005; Benn et al.,
47 2009). Given a supply of water to the bed, this theory has the potential to explain rapid surge motion
48 and coincident increases in basal water pressure, at least in glaciers with rigid beds (Kamb et al., 1985).
49 Indeed, observations of a subglacial flood that occurred during, but did not initiate, a surge suggest that
50 the basal hydrological system was likely inefficient during the surge and became channelized just prior
51 to surge termination (Bjornsson, 1998; Round et al., 2017). However, surges are often observed to begin
52 in late fall or winter, when surface meltwater supplies are limited (Kamb et al., 1985; Pritchard et al.,
53 2005; Echelmeyer et al., 1987; Roush et al., 2003; Bevington and Copland, 2014; Dunse et al., 2015). As
54 noted by Kamb (Kamb, 1987), often credited with introducing hydrological switching as an incipient surge
55 mechanism, surge onset in the absence of surface meltwater flux may require an incipient surge mechanism
56 beyond a switch from an efficient to an inefficient basal hydrological system. Furthermore, observations
57 of numerous surge-type glaciers in Iceland show that jökulhaups, or subglacial floods, do not cause surges
58 despite massive, rapid increases in basal water flux that characterize jökulhaups (Björnsson et al., 2003),
59 and it remains unclear if hydrological models derived under the assumption of rigid, impermeable beds are
60 applicable to glaciers with till-covered beds. In any case, hydrological models have not explained the spatial
61 distribution of surge-type glaciers and it seems unlikely that such models can explain why most surge-type
62 glaciers reside on deformable beds. So while the connection between surging and subglacial hydrology may
63 be robust, the causal link between the efficiency of the basal hydrological system and surge motion remains
64 unclear.

65 Another model of glacier surges, first advocated by Robin (Robin, 1955), contends that sediment un-
66 derlying a polythermal glacier may freeze during the quiescent phase, strengthening the bed, similar to
67 binge-purge models for Heinrich events (MacAyeal, 1993; Robel et al., 2013; Meyer et al., 2019). As ice
68 collects in an upstream reservoir, the thickening ice increases the overburden pressure at the bed, resulting
69 in a corresponding decrease in the melting temperature of ice that can cause the bed to thaw and, subse-
70 quently, weaken. Warm, weakened beds facilitate basal slip, resulting in frictional heating that melts basal
71 ice. Melted ice further lubricates the bed leading to enhanced basal slip and more heating, thereby driving
72 a positive thermal feedback loop (Fowler et al., 2001; Clarke, 1976; Clarke et al., 1977). Because thermal
73 control of glacier sliding requires ice to freeze to the bed, it cannot explain surging in temperate glaciers, in
74 which the ice is at the melting temperature and is unable to freeze to the bed. Recent observational work
75 shows that at least some surges in polythermal glaciers initiate in temperate zones, suggesting further limi-
76 tations on the applicability of thermal instability to incipient surge motion (Sund et al., 2014; Wilson et al.,
77 2014) and indicating that thermal instability is not a universal surge mechanism (Clarke, 1976).

78 The prevalence of till layers beneath surge-type glaciers suggests that changes in the mechanical prop-
79 erties of till caused by dilation and variable pore water pressure are a promising complement to the previous
80 models of incipient surge mechanisms, which assume rigid, impermeable beds (Benn et al., 2019; Thøgersen
81 et al., 2019). It would be difficult to overstate the complexity of granular mechanics in subglacial till (Clarke,
82 1987), which is especially pronounced where the till contains coarse clasts, where ice at the ice-bed inter-
83 face is laden with debris (Rempel, 2008; Zoet et al., 2013; Meyer et al., 2018), where the ice slides over the
84 ice-till interface (Zoet et al., 2013; Zoet and Iverson, 2016, 2018), where clasts frozen into the ice can plow

85 through the till (Thomason and Iverson, 2008), and where the till is mobilized during surging (Iverson et al.,
 86 2017). Even within a relatively simple layer of near-homogeneous sediment, we may expect multiple mech-
 87 anisms to contribute to till deformation at any given time, including grain boundary sliding, granular flow
 88 from comminution and grain rolling, and compaction and dilation caused by shearing (Davis and Selvadurai,
 89 2002; Fowler, 2003). Developing models that capture all of these mechanisms is an active area of research,
 90 and we know of no current models that account for all mechanisms in a manner that satisfyingly elucidates
 91 the underlying physics. Despite these challenges, notable surge models for glaciers with deformable beds
 92 have been proposed by other authors. Truffer et al. (Truffer et al., 2000, 2001) inferred till mobilization as
 93 a surge mechanism from direct observations of till deformation beneath a surge-type in Alaska. Woodward
 94 et al. (Woodward et al., 2003) proposed a conceptual model based on ice penetrating radar surveys of a
 95 surge-type glacier in Svalbard that indicated imbricate thrust faulting. And Clarke (Clarke, 1987) devel-
 96 oped a physical framework for subglacial till based in part on critical state soil mechanics and an assumed
 97 viscoplastic rheology for saturated subglacial till.

98 Motivated in part by these models for surging in glaciers with deformable beds, we present a new
 99 physical model that leverages the mechanical properties of granular materials to help explain incipient surge
 100 motion in the absence of additional surface meltwater flux and frozen beds. Our model is informed by
 101 studies of soil mechanics and earthquake nucleation and slow-slip events on tectonic faults containing water-
 102 saturated gouge. Gouge and glacial till are mechanistically comparable materials in that both derive their
 103 strength from a fine-grained matrix (Clarke, 1987) and, in the cases of fault breccia and till, may feature
 104 coarse clasts (Moore and Iverson, 2002). Regardless of the presence of coarse clasts, the load is carried by
 105 the fine-grained matrix. Laboratory experiments on fault gouge and till indicate that these materials have
 106 elastic-plastic rheologies with yield stresses defined by the normal effective stress (the difference between
 107 overburden and pore fluid pressure) and the tendency of the till to undergo internal frictional slip along
 108 grain boundaries (Fowler, 2003; Dieterich, 1979; Ruina, 1983; Kamb, 1991; Kilgore et al., 1993; Iverson
 109 et al., 1998; Tulaczyk et al., 2000a; Hooke, 2005; Iverson, 2010; Iverson and Zoet, 2015). Shear strength
 110 is a function of the rate of shearing within the till (hereafter called basal slip rate for glacier applications)
 111 and the shear history of the till. Accounting for shear history is important because shearing can cause
 112 either dilation or compaction of granular materials, depending on the state of consolidation in the material
 113 (Lambe and Whitman, 1969). Dilation has been identified through theory and observation as an important
 114 component controlling basal slip rates for glaciers in Svalbard and Alaska, ice caps in Iceland, and ice
 115 streams in Antarctica (Woodward et al., 2003; Truffer et al., 2001; Kamb, 1991; Tulaczyk et al., 2000a,b;
 116 Fuller and Murray, 2002; Robel et al., 2014, 2016), and here we seek to better understand the role of till
 117 compaction and dilation in incipient surge motion by developing a simple model that captures the relevant
 118 physical processes.

119 2 Model derivation

120 Consider a glacier with length ℓ , thickness h , and constant width $2w$, where $h \ll w \ll \ell$. Let us define a
 121 coordinate system oriented such that x is along flow, y is across flow in a right-handed configuration, and z
 122 is downward along the gravity vector (Fig. 1). Assume that ice thickness varies along-flow and is constant
 123 across-flow such that $h = h(x)$.

124 Water-saturated till underlies the glacier. We divide the till into two layers separated by a *décollement*:
 125 the top layer is deformable with thickness h_s and pore water pressure p_w , while the lower layer is a stationary,
 126 non-deforming half-space with pore water pressure $p_{w\infty}$. Aside from strain rate, pore water pressure, and
 127 otherwise stated properties, all physical properties of the till are assumed to be the same in both layers.
 128 Our idealized glacier has a subglacial hydrological system that, like any glacier, evolves due to changes in
 129 meltwater flux and basal slip rate (Schoof, 2010; Hewitt, 2013; Werder et al., 2013). Here we assume that
 130 both the state of the hydrological system and the basal water flux are accounted for in p_{w_r} , the water pressure

131 within the hydrological system, depicted as a reservoir in the system diagram (Fig. 1).

132 We assume that basal slip is due entirely to deformation of the upper till layer, meaning that p_{w_r} only
 133 influences ice flow through its influence on p_w . We make this simplifying assumption in spite of the fact that
 134 p_{w_r} may cause sliding of the ice relative to the bed (Hewitt, 2013; Lliboutry, 1968; Kamb, 1970; Fowler,
 135 1987a; Schoof, 2005) because our focus is on how the mechanical properties of till might induce surging
 136 in the absence of externally sourced meltwater flux. Unless there is a significant flux of meltwater into
 137 the subglacial hydrological system, an unlikely scenario during winter, p_{w_r} should remain approximately
 138 constant in time when averaged over a spatial scale of order the ice thickness. This assumption of nearly
 139 constant wintertime p_{w_r} is merely conceptual and is not a necessary condition in the subsequent derivation
 140 because time-varying p_{w_r} is accounted for in the model. Indeed, in future work, subglacial hydrological
 141 models could be readily bolted onto the model presented here. For simplicity, we ignore potential changes
 142 in pore water pressure caused by plowing particles (Zoet et al., 2013; Thomason and Iverson, 2008), and
 143 begin our study at the glacier bed with an exploration of till mechanics.

144 2.1 Mechanical properties of till

145 We adopt a phenomenological model for the mechanical strength of till that depends on basal slip rate u_b
 146 and the state of the subglacial till θ . This rate-and-state friction model accounts for instantaneous basal slip
 147 rate and, importantly, basal slip history, and was derived to explain numerous laboratory measurements of
 148 sliding on bare rock and granular interfaces. Rate-and-state friction is widely used in studies of earthquake
 149 nucleation and slow-slip events on tectonic faults, and gives the instantaneous shear strength of subglacial
 150 till as (Dieterich, 1979; Ruina, 1983)

$$\tau_t = N\mu = N \left[\mu_n + a \ln \left(\frac{u_b}{u_{b_n}} \right) + b \ln \left(\frac{\theta u_{b_n}}{d_c} \right) \right], \quad (1)$$

151 where μ_n is the coefficient of nominal internal friction, d_c is a characteristic slip displacement, u_{b_n} is a
 152 constant reference velocity, and the constants a and b are material parameters that define the magnitude of
 153 the direct (velocity) and evolution (state) effects, respectively. As we will discuss, b is important for this
 154 study at it encodes the effect of dilation on the bulk friction coefficient μ . In our idealized glacier geometry,
 155 the bed is horizontal and effective normal stress is equal to effective pressure, defined as

$$N = p_i - p_w, \quad (2)$$

$$p_i = \rho_i g h, \quad (3)$$

156 where ρ_i is the mass density of ice, g is gravitational acceleration, p_i is the ice overburden pressure, and p_w
 157 is the pore water pressure within the till.

158 Rate-and-state friction has received attention in studies of the ice-bed interface (Thøgersen et al., 2019;
 159 Zoet et al., 2013; Zoet and Iverson, 2018; Lipovsky and Dunham, 2017; McCarthy et al., 2017) and is widely
 160 studied for slip on tectonic faults containing gouge (Rice, 1983; Segall and Rice, 1995, 2006; Chen et al.,
 161 2017), a material mechanistically similar to till (Rathbun et al., 2008). Though distinct in many respects,
 162 earthquakes and glacier surges are analogous in the sense that both involve long quiescent periods and
 163 relatively short activation timescales. Slow-slip on tectonic faults are particularly relevant to studying glacier
 164 surges because of their comparable slip durations and slow slip rates compared with major earthquakes
 165 (Segall and Rice, 2006; Segall et al., 2010). Incipient motion in both earthquakes and glacier surges is
 166 brought on by excess applied stress relative to frictional resistance. While stresses and displacement rates
 167 are orders of magnitude higher in earthquakes than in glaciers, the experimentally verified rate-and-state
 168 friction model is applicable to glacier surges as there is no known lower bound on velocity for the model to
 169 be valid (Dieterich, 2007).

170 When till is deformed, individual grains are mobilized by cataclastic flow (which includes grain rolling
 171 and boundary sliding), dilation, and comminution. Under small displacements, the granular structure of the
 172 till is related to the pre-deformed structure, meaning that the till essentially remembers its prior state. Mem-
 173 ory is represented by the state variable θ , and is lost as the glacier slips over a characteristic displacement
 174 d_c . Steady state till shear strength occurs when state evolution ceases ($\dot{\theta} = 0$) and is defined as

$$\hat{\tau}_t = N \left[\mu_n + (a - b) \ln \left(\frac{\hat{u}_b}{u_{b_n}} \right) \right], \quad (4)$$

175 where $\hat{u}_b = d_c/\hat{\theta}$ is the steady state basal slip rate. (Hereafter, hatted values indicate steady state for the
 176 respective variable.) As we shall soon see, d_c is the slip distance over which state (and porosity) evolve,
 177 but it has also been interpreted as the slip distance at which the (rate-weakening) stress reduces to the
 178 residual stress (Palmer and Rice, 1973). Computational and microphysical studies have concluded that d_c is
 179 proportional to the thickness of the deforming layer (Chen et al., 2017; Marone and Kilgore, 1993; Marone
 180 et al., 2009), which can be expected to be of order 0.1–1 m in subglacial till and varies with permeability
 181 (Iverson et al., 1998; Damsgaard et al., 2015). Other factors influencing d_c include grain size and porosity
 182 (Chen et al., 2017).

183 State, θ , has dimensions of time. It has been taken to represent the product of the contact area and
 184 intrinsic strength (quality) of the contact (Ampuero and Rubin, 2008), but also has been interpreted as
 185 the average age of contacts between load-bearing asperities (Dieterich and Kilgore, 1994). Under either
 186 interpretation, state is expected to evolve as a function of time, slip, and effective normal stress (Dieterich,
 187 1979; Dieterich and Kilgore, 1994; Dieterich, 1981; Rice and Ruina, 1983). To represent the evolution of θ ,
 188 we adopt what is commonly referred to as the slip law (Ruina, 1983)

$$\dot{\theta} = -\frac{\theta u_b}{d_c} \ln \left(\frac{\theta u_b}{d_c} \right), \quad (5)$$

189 which dictates that state evolves only in the presence of slip. The only stable steady state in Eq. 5 exists at
 190 $\theta = d_c/u_b$; when $u_b > 0$, θ always tends toward the stable steady state. Increasing u_b beyond d_c/θ , through
 191 enhanced surface meltwater flux, calving, or other external forcing, will reduce θ over time. Similarly, when
 192 $u_b < d_c/\theta$, θ will increase toward steady state. In the next section we show that changes in θ are brought
 193 about through till compaction and dilation. As such, θ accounts for the basal slip history and plays a key
 194 role in determining bed strength and the response of bed strength to shear and external forcing.

195 2.2 Pore water pressure

196 Till shear strength is proportional to effective pressure (Eg. 1), the difference between overburden and pore
 197 water pressure (Eq. 2). Assuming that the mass density of ice remains constant, effective pressure can only
 198 vary during surges due to changes in ice thickness and pore water pressure. Pore water pressure is linked to
 199 till compaction and dilation through changes in the effective till porosity. Thus, if we assume that the till is
 200 always saturated, then the rate of change of water mass per unit volume within the till is given as

$$\dot{m}_w = \rho_w \dot{\phi}, \quad (6)$$

201 where ϕ is the (dimensionless) effective till porosity, defined as the ratio of pore volume to total volume, and
 202 ρ_w is the density of water. In this section, we seek to understand the rate of change in pore water pressure
 203 as a function of basal slip rate under the basic assumptions that water is incompressible over the range of
 204 reasonable subglacial pressures and that frictional heating at the ice-bed interface and plastic dissipation
 205 within the till are negligible.

206 **2.2.1 Evolution of porosity**

207 Assuming that individual grains in the till are rigid, strain within the till will be accommodated by changes
 208 in porosity. Adopting an elastic-plastic model for the deformation of granular till, wherein the total strain
 209 is equal to sum of the elastic and plastic strains, we separate porosity changes into a plastic component, $\dot{\phi}_p$,
 210 and an elastic component $\dot{p}_w\beta$ such that (Segall and Rice, 1995; Walder and Nur, 1984)

$$\dot{\phi} = \dot{p}_w\beta + \dot{\phi}_p, \quad (7)$$

where

$$\beta = \frac{\partial\phi}{\partial p_w} = \frac{\epsilon_e (1 - \phi)^2}{N} \quad (8a,b)$$

211 is the till compressibility and ϵ_e is the elastic compressibility coefficient, taken to be in the range $\epsilon_e \sim 10^{-3}$ –
 212 10^{-1} (Minchew, 2016). Following work by Segall and Rice (Segall and Rice, 1995) and Segall et al. (Segall
 213 et al., 2010) on slow-slip events on tectonic faults, we take the plastic component of porosity to have the
 214 same form as the evolution component of the rate-and-state model for till shear strength (Eq. 1), namely

$$\phi_p = \phi_c - \epsilon_p \ln \left(\frac{\theta u_{bn}}{d_c} \right), \quad (9)$$

215 where ϕ_c is a (constant) characteristic porosity and ϵ_p is a dilatancy coefficient, a dimensionless parameter
 216 hereafter assumed constant and in the range $10^{-4} \leq \epsilon_p \leq 10^{-2}$ (Segall et al., 2010). We note that the only
 217 sensitivity in our model to the absolute value of ϵ_p is to the evolution of porosity; surge behavior, the main
 218 focus of this study, is influenced only by the ratio ϵ_p/β , which represents the relative importance of each term
 219 in Eq. 7. By adopting Eq. 9, we are assuming that plastic deformation of the till is completely determined
 220 by changes in state, θ , the only variable in Eq. 9. This assumption is physically justifiable: irreversible
 221 changes in porosity necessitate a change in the average age of granular contacts and, equivalently, a change
 222 in the product of the contact area and quality, both of which are the physical interpretations of state discussed
 223 above. Differentiating Eq. 9 in time yields

$$\dot{\phi}_p = -\epsilon_p \frac{\dot{\theta}}{\theta}, \quad (10)$$

224 an expression that indicates that shearing causes till to compact ($\dot{\phi}_p < 0$) when θ is below steady state
 225 ($\theta < d_c/u_b$) and to dilate when θ is above steady state. Such behavior is consistent with observations of the
 226 response of over- and under-consolidated soils to shear (Lambe and Whitman, 1969). As we will show, the
 227 relationship between plastic till deformation and state will give rise to rich mechanical relationships between
 228 compaction, dilation, and shearing, as is expected from sediments.

229 **2.2.2 Evolution of pore water pressure**

230 Let us now consider water flux in the till in response to changes in porosity and sources outside the till shear
 231 layer. The rate of change of water mass is given by plugging the expressions for the total rate of change in
 232 porosity (Eq. 7) and the rate of irreversible (plastic) change in porosity (Eq. 10) into the expression for the
 233 rate of change in mass per unit volume (Eq. 6) yielding

$$\dot{m}_w = \rho_w \dot{p}_w\beta + \rho_w \epsilon_p \frac{u_b}{d_c} \ln \left(\frac{\theta u_b}{d_c} \right). \quad (11)$$

234 Conservation of water mass gives

$$\frac{\partial q_w}{\partial z} + \dot{m}_w = 0, \quad (12)$$

235 where q_w is the water mass flux and we have assumed horizontal gradients in water pressure are negligible
 236 compared with vertical gradients. Taking the basal ice to be impermeable requires water flux to be entirely
 237 into and out of the bed. Under these conditions, Darcy's law is given as

$$q_w = -\frac{\rho_w \gamma_h}{\eta_w} \frac{\partial p_w}{\partial z}, \quad (13)$$

238 where γ_h is the till permeability and η_w is the dynamic viscosity of water. Combining Eqs. 11–13 under the
 239 assumption that till permeability is spatially constant and independent of porosity gives

$$\dot{p}_w = \kappa_h \frac{\partial^2 p_w}{\partial z^2} + \frac{\epsilon_p \dot{\theta}}{\epsilon_e \theta} \frac{N}{(1 - \phi)^2}, \quad (14)$$

240 where

$$\kappa_h = \frac{\gamma_h}{\eta_w \beta}, \quad (15)$$

241 is the hydraulic diffusivity of the deforming till layer. Measurements of hydraulic diffusivity in till give
 242 a range for κ_h of approximately 10^{-9} – 10^{-4} m²/s, with a strong sensitivity to clay content (Iverson et al.,
 243 1997; Cuffey and Paterson, 2010). We take constant effective permeability to be a reasonable first approxi-
 244 mation given the small change in permeability under glaciologically relevant pressures and strains found in
 245 discrete element modeling studies (Damsgaard et al., 2015). A more general treatment of pore water pres-
 246 sure evolution would include a porosity-dependent permeability in place of a constant effective permeability
 247 — for example, the Kozeny-Carman model used by (Clarke, 1987). We reserve this additional complexity
 248 for future work as our simple model retains the salient physical processes.

249 Shearing in till concentrates in a thin, multi-layer zone that is typically several centimeters thick (Tu-
 250 laczyk et al., 2000a; Boulton and Hindmarsh, 1987; Boulton et al., 2001; Iverson and Iverson, 2001). We
 251 therefore approximate

$$\frac{\partial^2 p_w}{\partial z^2} = \frac{p_{w_\infty} - 2p_w + p_{w_r}}{h_s^2}, \quad (16)$$

252 where h_s is the thickness of the shear zone in the till, p_{w_∞} is the water pressure in the underlying permeable
 253 half space, and p_{w_r} is the water pressure in the basal hydrological system (Fig. 1). With this approximation,
 254 Eq. 14 becomes

$$\dot{p}_w = \frac{p_{w_\infty} - 2p_w + p_{w_r}}{t_h} + \frac{\epsilon_p \dot{\theta}}{\epsilon_e \theta} \frac{N}{(1 - \phi)^2}, \quad (17)$$

255 where the first term represents Darcian flow into and out of the deforming till layer and the second term
 256 represents dynamical (dilation-driven) changes in pore water pressure. The Darcy-flow component of pore
 257 water pressure evolution is inversely proportional to the characteristic diffusive timescale for pore water in
 258 the deforming till layer

$$t_h = \frac{h_s^2}{\kappa_h}. \quad (18)$$

259 To simplify the analysis, we hereafter take t_h to be constant, thereby ignoring the dependence of κ_h and h_s
 260 on effective pressure N and porosity ϕ . We justify this simplification by noting that κ_h (Eq. 15) and till
 261 thickness h_s roughly scale as N , though a detailed analysis of the relation between h_s and N is beyond the
 262 scope of this work (Clarke, 1987). Assuming $h_s \sim N$ and $\kappa_h \sim N$, $t_h \sim N$ to a reasonable approxima-
 263 tion and therefore should retain the same order of magnitude during incipient surge motion. Similarly for
 264 permeability, where compaction-driven reductions in permeability will induce relatively small (factor of 2)
 265 decreases in thickness h_s (Damsgaard et al., 2015). Such small changes are unlikely to dramatically alter
 266 the dynamics of surge motion captured here, and we leave for future work a more detailed analysis involving
 267 variable t_h .

268 From the second term in Eq. 17, we can see that the sign of the dynamical (or dilation-driven) component
 269 of \dot{p}_w is determined by the state of the till relative to steady state. When state, θ , is below (above) steady
 270 state and $t_h > 0$, pore water pressure will increase (decrease) until steady state is achieved. These changes
 271 in pore water pressure are entirely due to changes in till porosity: compaction ($\dot{\phi}_p < 0$) results in faster rates
 272 of change in the dynamical component of water pressure because $\epsilon_p \dot{\theta} N / [\epsilon_c \theta (1 - \phi)^2] = -\dot{\phi}_p / \beta$. Whether
 273 p_w increases or decreases following step changes in basal slip rate depends on the whether the ratio $\theta u_b / d_c$
 274 is greater than or less than unity.

275 2.3 Basal slip acceleration

276 Glacier ice is an incompressible viscous fluid in laminar flow, and the momentum equation, incompressibil-
 277 ity condition, and continuity equation, respectively, take the forms

$$0 = \frac{\partial \tau_{ij}}{\partial x_j} - \frac{\partial \tilde{p}}{\partial x_i} + \rho_i g \delta_{iz}, \quad (19)$$

$$0 = \frac{\partial u_i}{\partial x_i}, \quad (20)$$

$$\dot{h} = \dot{M} - \frac{\partial}{\partial x_i} (h \bar{u}_i), \quad (21)$$

278 where u_i is the ice velocity vector, \bar{u}_i is the depth-averaged ice velocity vector, τ_{ij} is the deviatoric stress
 279 tensor, δ_{ij} is the Kronecker delta, \tilde{p} is the mean isotropic ice stress (pressure), \dot{M} is the total surface mass
 280 balance (which includes surface and basal mass balance and is positive for mass accumulation), and we em-
 281 ploy the summation convention for repeated indices. To simplify our analysis, we neglect vertical shearing
 282 in the ice column, and adopt a depth-integrated momentum equation (often referred to as the shallow shelf
 283 approximation) (MacAyeal, 1989)

$$2 \frac{\partial}{\partial x} (h \tau_{xx}) + \frac{\partial}{\partial y} (h \tau_{xy}) + \tau_b = \tau_d, \quad (22)$$

284 where τ_{xx} is the extensional deviatoric stress, τ_{xy} the lateral shear stress, and we have neglected the trans-
 285 verse normal (deviatoric) stress τ_{yy} . In some surge-type glaciers, vertical shearing may be the dominant flow
 286 regime during the quiescent phase, while basal slip is the dominant flow regime during the surge phase. Eq.
 287 22 is valid only when basal slip is dominant, and thus a model of basal slip acceleration derived from Eq.
 288 22 may not fully detail glacier flow during incipient surge acceleration in some glaciers. Nevertheless, this
 289 simplification is reasonable because the focus of this work is on till mechanics and the flow model based on
 290 Eq. 22 will represent the salient processes of nascent surge acceleration. We reserve for future work a more
 291 detailed analysis that retains more components of the stress divergence and is able to capture the transition
 292 from vertical-shear-dominated flow to basal-slip-dominated flow.

293 Force balance dictates that basal shear traction cannot exceed the lesser of applied stress and yield stress
 294 of the till, giving rise to the relation (Iverson et al., 2017; Minchew et al., 2016)

$$\tau_b = \min(\tau_d, \tau_t), \quad (23)$$

295 where $\tau_t = \mu N$ is the till shear strength (Eq. 1) and the gravitational driving stress is defined as

$$\tau_d = \rho_i g h \alpha \quad (24)$$

296 where α is the ice surface slope, assumed small such that $\sin(\alpha) \approx \alpha$. Recall that we are focusing on the
 297 case in which rapid flow during the surge is accommodated primarily by deformation of the bed, giving rise
 298 to the relations $\tau_b = \tau_t$ and $u_s \approx u_b$.

299 Let us now focus only on the region where the surge is initiated and assume the areal extent of incipient
 300 surge motion is large enough to make the gradient of longitudinal stress (first term in Eq. 22) negligible
 301 during the nascent surge phase. Taking ice to be shear-thinning fluid, the constitutive relation, commonly
 302 known as Glen’s law (Glen, 1955), is

$$\dot{\epsilon}_e = A\tau_e^n, \quad (25)$$

303 where $\dot{\epsilon}_e = \sqrt{\dot{\epsilon}_{ij}\dot{\epsilon}_{ij}/2}$ is the effective strain rate, $\tau_e = \sqrt{\tau_{ij}\tau_{ij}/2}$ is the effective deviatoric stress, the rate
 304 factor A is a scalar, and the stress exponent is $n = 3$. Hereafter, A and n are assumed constant. Under
 305 our prior assumptions, $2\dot{\epsilon}_e \approx \partial u_b/\partial y$ and $\tau_e \approx \tau_{xy}$. Integrating the reduced form of Eq. 22 twice along y
 306 subject to the symmetry condition $\tau_{xy} = 0$ at the centerline and no-slip condition at the margins gives the
 307 centerline basal slip rate

$$u_b = u_r \left[\alpha - \mu \left(1 - \frac{p_w}{p_i} \right) \right]^n, \quad (26)$$

308 where

$$u_r = \frac{2A(\rho_i g)^n}{n+1} w^{n+1}, \quad (27)$$

309 is a reference velocity. Taking u_r and w to be constants and differentiating Eq. 26 with respect to time yields
 310 an expression for acceleration in basal slip

$$\dot{u}_b = nu_b \left[\frac{\dot{\alpha} - \mu \frac{p_w}{p_i} \left(\frac{\dot{h}}{h} - \frac{\dot{p}_w}{p_w} \right) - b \frac{\dot{\theta}}{\theta} \left(1 - \frac{p_w}{p_i} \right)}{\alpha + (an - \mu) \left(1 - \frac{p_w}{p_i} \right)} \right], \quad (28)$$

311 where the rates of change in glacier geometry (\dot{h} and $\dot{\alpha}$), pore water pressure (\dot{p}_w), and state ($\dot{\theta}$) all contribute
 312 to the basal slip acceleration, along with instantaneous geometry (h and α), pore water pressure (p_w), state
 313 (θ), and basal slip rate (u_b). Note that the conditions $\tau_d > \tau_b$ and $\tau_b = \tau_t$, discussed and imposed earlier in
 314 this section, ensure that the denominator in Eq. 28 is always greater than zero.

315 Eq. 28 is the central result of this study. This formula describes the dependence of surge acceleration
 316 on glacier geometry, pore water pressure, and the properties of the till. The terms in the numerator can be
 317 related to the processes of interest during the surge. Namely, the first term in the numerator ($\dot{\alpha}$) essentially
 318 represents the rate of change in the gravitational driving stress. The second term in the numerator captures
 319 the evolution of effective pressure (N), which governs the shear strength of the bed. The third and final
 320 term in the numerator accounts for the influence of dilation on the internal friction coefficient of the till. We
 321 spend the remainder of this study investigating the influence of the various physical processes represented
 322 in Eq. 28.

323 3 Results

324 Since shear strength of the till is the governing factor in surge motion and is defined by three variables
 325 (overburden pressure p_i , pore water pressure p_w , and the internal friction coefficient μ), we present the
 326 results in three sections. In the first section, we discuss the evolution of pore water pressure following an
 327 increase in basal slip rate. Second, we consider the acceleration of basal slip for a glacier with a fixed
 328 geometry (*i.e.*, fixed overburden pressure). Lastly, we explore the full model, which allows for variations in
 329 pore water pressure, glacier geometry, and internal friction coefficient for till.

3.1 Evolution of pore water pressure

Pore water pressure in the deforming till layer evolves due to dilation and compaction of the till as well as through the exchange of water between the deforming till layer, the subglacial hydrological system, and the stagnant till layer that underlies the deforming layer (Eq. 17 and Fig. 2). In our model, the pressures in the stagnant till layer and the subglacial hydrological system are assumed constant in time, and the flow of water into or out of the deforming till layer is described by Darcy’s law (Eq. 13). Using the parameter values given in the caption of Fig. 2, we integrate Eqs. 5, 7, and 17 forward in time from the initial conditions $u_{b_0} = 10$ m/yr, $\phi_0 = 0.1$, $\theta_0 = d_c/u_{b_0}$, and $p_{w_0} = p_{w_r} = p_{w_\infty}$ using the variable-coefficient ordinary differential equation (VODE) solver implemented in SciPy (version 1.3.1), an open-source Python toolkit (Jones et al., 2018).

The results shown in Fig. 2 illustrate how the evolution of pore water pressure p_w following a step increase in basal slip rate is influenced by the hydraulic diffusion timescale of the deforming till layer (t_h) and the relative values of the elastic (ϵ_e) and plastic (ϵ_p) compressibility coefficients. Note that because we hold t_h fixed in time, only the relative compressibility ratio ϵ_e/ϵ_p influences pore water pressure, not the absolute values of ϵ_e and ϵ_p . All cases shown in Fig. 2 start at steady state and indicate initial decreases in pore water pressure p_w in response to till dilation followed by a return to steady state ($p_{w_0} = p_{w_r} = p_{w_\infty}$) via Darcian flow over a timescale proportional to the diffusion timescale. The minimum pore water pressure is determined by the diffusion timescale t_h and the relative compressibility ϵ_e/ϵ_p . For a given relative compressibility, longer diffusion timescales, corresponding to lower till permeabilities, lead to a greater drop in pore water pressure (Fig. 2, upper panel). For a given diffusion timescale, smaller values of relative compressibility, which indicate stronger dilatancy of the till relative to poroelastic effects, result in greater drops in pore water pressure (Fig. 2, lower panel).

3.2 Acceleration with fixed ice thickness

We now consider glacier acceleration. As a first step, we simplify our analysis by assuming that the timescale of interest is longer than the timescale for pore water diffusion ($t > t_h$) but short enough to allow us to reasonably neglect changes in glacier geometry. While it can be argued that this condition may be physically contrived in some cases, it is useful for exploring surge dynamics and the behavior of the till in the absence of some complicating factors (in the next section we will allow glacier geometry to evolve). After fixing glacier geometry by imposing $\dot{h} = 0$ and $\dot{\alpha} = 0$ at all times, we solve the system of equations defined by Eqs. 5, 7, 17, and 28. For all results discussed here, we prescribe as the initial velocity $u_b = 1.1\hat{u}_b$ at $t = 0$, where $\hat{u}_b = 10$ m/yr, and set the initial values for all other variables to their respective steady state values. The system of equations is stiff, and therefore, we integrate forward in time using an implicit Runge-Kutta method — specifically the Radau IIA fifth-order method — implemented in SciPy (version 1.3.1).

In the cases shown in Fig. 3, we focus on the influences of a range of viable evolution effects (b values; indicated by line intensity and thickness) and different hydraulic diffusion timescales (t_h ; indicated by colors). Aside from b and t_h , all parameters are the same for all cases and are listed in the Fig. 3 caption. Note that $a = 0.013$, so in terms of the till friction coefficient μ , the cases shown in Fig. 3 are both rate-weakening ($a < b$; solid lines) and rate-strengthening ($a > b$; dashed lines).

The most notable feature in all cases shown in Fig. 3 is the lack of unstable acceleration. Steady state speed is governed by the steady state shear strength of till (Eq. 4) and is therefore sensitive to the rate-and-state parameters ($a - b$) and μ_n . Since the direct effect (a) is constant all cases in Fig. 3, increasing the evolution effect (b) leads to a greater steady state stress drop and faster steady state basal slip rate due to the increasingly negative value ($a - b$). The steady state values for all state variables are independent of the diffusion timescale t_h and characteristic slip length d_c . The primary influences of t_h and d_c are on the time the system take to reach steady state and the peak change in pore water pressure. These results show that

375 the system tends to steady state over a characteristic timescale that scales with the (dimensionless) hydraulic
 376 transmittance

$$\psi_0 = \frac{\epsilon_p \hat{u}_{b_0} t_h}{\epsilon_e d_c} \quad (29)$$

377 defined as the ratio of the hydraulic diffusion timescale t_h to the timescale for dilation-driven changes in
 378 pore water pressure $d_c \epsilon_e / (\epsilon_p u_{b_0})$. The dependence on ψ_0 of the time to steady state is indicated in Fig. 3 by
 379 noting that the only term in ψ_0 that changes between the difference cases is the hydraulic diffusivity κ_h (and,
 380 consequently, t_h). The time axes in Fig. 3 are normalized by $d_c \epsilon_e / (\epsilon_p u_{b_0})$, the timescale for dilation-driven
 381 changes in pore water pressure to help show that model realizations in which the diffusion timescale t_h is an
 382 order of magnitude longer, take an order of magnitude longer time to evolve to steady state. As we show in
 383 the next section, the time required to reach steady state is a crucial factor governing whether or not a glacier
 384 surges.

385 The behavior of the model in the absence of changes in glacier geometry (Fig. 3) provides further insight
 386 that help explain some of the results of the full model presented in the next section. For instance, the till
 387 dilates in all cases due to initial step and subsequent changes in basal slip rate (Fig. 3). The amplitude of
 388 the change in till porosity scales with the evolution parameter b , with larger values of b resulting in greater
 389 dilatancy. As seen in the previous section, higher dilatancy results in a larger drop in pore water pressure
 390 as the glacier accelerates. Dilatancy also drives a reduction in the internal friction coefficient of till, as a
 391 dilated till provides less resistance to shearing due to reduced contact areas between grains. This drop in the
 392 internal friction coefficient commensurately reduces the shear strength of the till.

393 3.3 Acceleration with variable ice thickness

394 Over longer timescales, dynamically driven changes in glacier geometry can be important, and we must
 395 consider the full expression given in Eq. 28. To do so, we approximate changes glacier geometry by
 396 recalling that h varies only in the along-flow (x) direction and focusing only on the central trunk of the
 397 glacier where across-flow variations in the depth averaged velocity vector \bar{u} can be neglected. Thus, the
 398 continuity equation (Eq. 21) becomes

$$\dot{h} = \dot{M} - \frac{\partial}{\partial x} (\zeta h u_s), \quad (30)$$

399 where $\zeta = \bar{u}/u_s$, \bar{u} is the depth-averaged glacier speed, and u_s is the glacier surface speed. Since we have
 400 taken ice to be a non-Newtonian viscous fluid, we have $(n+1)/(n+2) \leq \zeta \leq 1$, where n is the stress
 401 exponent in the constitutive relation for ice (Eq. 25). In this study, we adopt the most common value for
 402 the stress exponent, $n = 3$, and we prescribe $\zeta = 1$ for consistency with the reduced momentum equation
 403 in Eq. 22 (when $\zeta = 1$, $u_s = u_b$). We further simplify the expression for dynamical thinning by neglecting
 404 extensional strain rates (consistent with the assumptions in §22.3), yielding

$$\dot{h} = \alpha \zeta (u_* - u_b), \quad (31)$$

where $u_* = \dot{M}/(\alpha \zeta)$ is the balance velocity. Finally, the rate of change in surface slope becomes

$$\dot{\alpha} = -\frac{\partial \dot{h}}{\partial x} \approx \frac{\dot{h} \alpha}{h} \quad (32a,b)$$

405 where Eq. 32b follows from the assumption of a parabolic surface profile for the glacier (Minchew, 2016).
 406 These approximations complete the quasi-1D model, and we solve Eqs. 5, 17, 28, 31, and 32 using the
 407 numerical solver described in §33.2.

408 The results, shown in Fig. 4, indicate markedly different behavior from the case where glacier geometry
 409 was held fixed (§33.2). Most notably, surging — defined here as an order of magnitude increase in basal slip

410 rate — occurs for some combinations of the evolution parameter b and diffusion timescale t_h . In particular,
 411 for our chosen parameters (given in the Fig. 4 caption), higher b values and longer t_h times result in surges.
 412 On the other hand, b values and t_h times too small and/or short to generate surge behaviors produce prosaic
 413 glacier dynamics (small b , short t_h) or abandoned surges (small b , long t_h), the latter of which we define
 414 as a period of rapid flow speeds (factor of two or more faster than quiescent speeds) that do not meet the
 415 definition of a surge, followed by a slowdown and evolution to steady state. To clarify the distinction: Initial
 416 acceleration is unstable in surges and stable in abandoned surges.

417 To explore the processes that govern whether a surge develops, is abandoned, or is essentially absent,
 418 let us focus on some illustrative cases shown in Fig. 4. We start with two prominent cases: those with
 419 the highest b values (and therefore the heaviest lines in Fig. 4) and different hydraulic diffusivities (*i.e.*, t_h
 420 values). The case with $b = 0.05$ and higher diffusivity (and, consequently, higher hydraulic permeability
 421 and shorter t_h), shown with the heavy red lines in Fig. 4, undergoes an abandoned surge, defined by a
 422 brief acceleration phase, resulting in a maximum velocity of approximately twice the steady state slip rate
 423 ($u_b/\hat{u}_{b0} \approx 2$), followed by deceleration and evolution to steady state. In this case, the glacier thins some-
 424 what, but the till tends to steady state before there is any marked change in the effective pressure at bed (N).
 425 The case with $b = 0.05$ and lower hydraulic diffusivity (heavy blue line) surges, with muted acceleration
 426 (relative to the case with higher hydraulic diffusivity) preceding a continual reduction in state, pore water
 427 pressure, ice thickness, and till internal friction coefficient. The rates of change in each of these values when
 428 the integration was terminated (at $u_b/\hat{u}_{b0} = 10$) show that the glacier would continue to accelerate in the
 429 absence of contravening processes, such as increases in extensional stresses, that are not considered in our
 430 model but could manifest in a natural glacier. It is important to note that the effective pressure N continually
 431 decreases despite reductions in pore water pressure p_w because of the dynamic thinning of the glacier. In
 432 other words, reductions in overburden pressure $p_i = \rho_i g h$ outpace reductions in pore water pressure p_w ,
 433 leading to a net decrease in $N = p_i - p_w$ that complements reductions in the friction coefficient μ , ensuring
 434 that basal drag ($\tau_b = \tau_t = N\mu$) diminishes in time. Sustained acceleration of the glacier unequivocally
 435 indicates that the decline of basal drag outpaces thinning-induced reductions in gravitational driving stress.

436 Other cases shown in Fig. 4 indicate the same basic behavior: till with higher values of hydraulic
 437 permeability allows for faster acceleration, which causes the till to evolve to steady state before significant
 438 thinning of the glacier can occur. Rates of acceleration and evolution to steady state are slower in less-
 439 permeable till, allowing rapid ice flow to persist for longer periods of time, facilitating dynamic thinning of
 440 the glacier. Longer timescales with relatively muted acceleration allow for thinning because dynamic glacier
 441 thinning scales as the time-integral of ice velocity (Eq. 31), meaning that longer periods of moderately rapid
 442 flow can produce more thinning than much short periods of somewhat faster flow. These results suggest that
 443 it is the reduction in overburden pressure p_i , and therefore effective pressure N , through dynamic thinning
 444 that is ultimately responsible for sustaining surge motion. The lack of unstable acceleration when glacier
 445 geometry is fixed in time (discussed in the previous section) and the manifestation of surging in cases of rate-
 446 strengthening friction coefficients (dashed lines in Fig. 4) both serve to highlight importance of dynamic
 447 thinning for sustaining surge motion.

448 The evolution of till porosity, as shown in Fig. 4, is markedly different from the case with fixed glacier
 449 geometry (previous section). Till consistently dilated when glacier geometry was fixed because effective
 450 pressure decreased then returned to steady state along with water pressure. But the dependence of the rate
 451 of change in till porosity on the effective pressure via β (Eqs. 7 and 8) results in net compression when we
 452 allow the glacier to thin. As effective pressure decreases due to thinning of the glacier, the sensitivity of
 453 the rate of change in porosity due to changes in pore water pressure become more pronounced. Since pore
 454 water pressure decreases in response to the evolution of till state (Eq. 17), the net effect is till compaction
 455 that lags reductions in pore water pressure.

456 The results discussed in this section indicate that the principal factors governing the surge behavior of a
 457 glacier are the hydraulic diffusion timescale of the deforming till layer, t_h , the relative compressibility ϵ_e/ϵ_p ,

458 and the evolution parameter b , the latter of which dictates the response of the internal friction coefficient
 459 to till dilation. We explore this parameter space in Fig. 5; except where indicated, model parameters
 460 are the same as for Fig. 4, and we use the same numerical solver. The results in Fig. 5 show that for
 461 any relative compressibility ϵ_e/ϵ_p , surge-type behavior is favored in glaciers with high b values and long
 462 diffusion timescales (*i.e.*, relatively impermeable beds). Higher b values imply a greater reduction in the
 463 internal friction coefficient of till (μ) in response to changes in porosity (and therefore, state), with rate-
 464 weakening values ($b > a$) resulting in a reduced steady state friction coefficient. Positive glacier acceleration
 465 is generally expected as the friction coefficient decreases in response to state evolution, causing surges to
 466 be favored at higher b values. As previously discussed, longer diffusion timescales (*i.e.*, lower hydraulic
 467 permeability) diminish the rate of porosity (state) evolution, and therefore, slows dilatant hardening effects.
 468 Thus, slow diffusion of pore water enables a longer acceleration period that allows time for dynamic glacier
 469 thinning to drive a net reduction in the effective pressure. Surge-type glaciers are more likely to manifest
 470 in tills that have a high relative compressibility, $\epsilon_e/\epsilon_p > 10$, as these higher values imply less dilatant
 471 hardening (the reduction in pore water pressure due to shearing; cf. Fig. 2).

472 The rich dynamical behavior illuminated in Fig. 5 is enhanced by the manifestation of regions (in the
 473 parameter space) of abandoned surges adjacent to the regions of surging behavior. Abandoned surge regions
 474 are indicated in Fig. 5 by maximum basal slip rates greater than the initial value ($u_{b_{max}}/\hat{u}_{b_0} > 2$, as shown
 475 in purple-to-red hues) and final basal slip rates less than the initial value ($u_{b_{final}}/\hat{u}_{b_0} < 0.5$, as shown in
 476 grey tones). Abandoned surges manifest only where b values are relatively large but not large enough to
 477 produce a surge and diffusion timescales are slightly too short to allow for a full surge. According to our
 478 results, it is possible for a glacier to exhibit abandoned surges for any value of ϵ_e/ϵ_p , but the region in the
 479 parameter space that produces abandoned surges increases with ϵ_e/ϵ_p (*i.e.*, as dilatant hardening decreases).

480 Two other remarkable and persistent features of the parameter space are worth highlighting. First, aban-
 481 doned surge regions are accompanied by an area of the parameter space that takes the shape of an airfoil
 482 containing points suitable for surge-type glaciers. In all cases, these airfoil features are isolated from the
 483 main region of surging, oriented at roughly the same angles in the parameter space, have long-axes lengths
 484 that scale nonlinearly with ϵ_e/ϵ_p , and have positions that shift toward higher t_h and smaller b as ϵ_e/ϵ_p in-
 485 creases. The boundaries of these features are diffuse in the direction of smaller t_h and b but feature sharp
 486 transitions in both max and final slip rates at higher t_h and b values. Second, the boundary separating the
 487 surging region from the non-surging and abandoned surge regions is sharp, rather than diffuse, suggesting
 488 the existence of a supercritical Hopf bifurcation at the (approximately) linear boundary between surging and
 489 non-surging in the t_h - b parameter space. As expounded on in the Discussion section, this sharp boundary
 490 and possible bifurcation illuminates some potential mechanisms that cause surging to switch on and off over
 491 longer (multi-centennial) timescales in given glacier system, and for surging glaciers to be relatively rare
 492 and geographically clustered. We reserve for future work detailed exploration of bifurcations in the system.

493 To better understand the features in Fig. 5, we further explore the dynamics in Fig. 6, which shows that
 494 small variations in b for fixed values of t_h and ϵ_e/ϵ_p lead to a range of responses. The parameter values repre-
 495 sented in Fig. 6 are shown with corresponding colors in Fig. 5. In order of decreasing b , we observe surging
 496 following the perturbation (blue line; $b = 0.03$), abandoned surging (orange line; $b = 0.028$), an abandoned
 497 surge followed by a surge at longer timescales (red line; $b = 0.026$), and slight dynamical variations (green
 498 and olive lines; $b \leq 0.024$). These transitions in dynamical behavior as a function of decreasing b can be
 499 understood in the context of changes in μ , the internal friction coefficient of the till. The sensitivity of μ to
 500 changes in state increases with b values, allowing for greater and more rapid reductions in the friction coef-
 501 ficient — and, by extension, the shear strength of the till, τ_t (lowest panel of 6) — at higher b values. Thus,
 502 higher b values lead to unstable acceleration immediately following the perturbation by allowing dynamic
 503 glacier thinning driven a net reduction in the effective pressure, further decreasing the shear strength of the
 504 till. Slightly smaller b values in the abandoned surge region result in slightly smaller changes in μ , which
 505 creates a situation that is unfavorable to surging because the acceleration in basal slip rate is sufficiently fast

506 to drive till evolution but not significant dynamic thinning of the glacier. As a result, the initial acceleration
 507 is facilitated by reductions in both the effective pressure and internal friction coefficient, but decreases in
 508 pore water pressure eventually outpace reductions in overburden pressure, resulting in an net increase in
 509 effective pressure (and τ_t) and ultimate stagnation of basal slip. Finally, a delayed surge manifests at median
 510 b values ($b = 0.026$ for $t_h = 2600$ days; red line in Fig. 6) due to trade-offs in basal slip acceleration, till
 511 dilation, and evolution of the internal friction coefficient. In this case, small initial decreases in μ driven
 512 by state evolution allow for basal slip acceleration, which drives the till toward steady state and ultimately
 513 increases state beyond the initial steady state value as the glacier slows. Since basal slip does not stagnate
 514 as it did in the previously discussed case, the till continues to evolve, eventually leading to compaction and
 515 commensurate increase in pore water pressure. This increase in pore water pressure drives a reduction in
 516 effective pressure that leads to glacier acceleration, which eventually becomes self-sustaining as the glacier
 517 thins and effective pressure drops.

518 We find good agreement between our model behavior and observations of surge motion in natural
 519 glaciers (Fig. 7). Our model reproduces both the timing and order of magnitude of the speedup with a
 520 range of values for the evolution coefficient b and diffusion timescale t_h . In Fig. 7 we show results using
 521 $b = 0.03$ and $t_h = 3000$ days and other parameters corresponding to values used in Figs. 3 and 4. Note
 522 that our focus in this study has been on the incipient acceleration phase of the surges, and simplifications
 523 in the model, namely the lack of an evolving subglacial hydrological system and consideration of exten-
 524 sional stresses in the momentum balance, prevent the model from decelerating (Benn et al., 2019). The
 525 agreement between our model and these data, however, is encouraging as it suggests that the dilation and
 526 glacier-thinning timescales we consider in our model do indeed work in concert to trigger glacier surges.

527 4 Discussion

528 At this point, we have derived and explored the behavior of a fundamentally new dynamical model of
 529 incipient surge motion that considers the mechanics of subglacial till and ice flow. Few comparable models
 530 exist in the literature, thus we endeavor to develop the simplest model capable of capturing the salient
 531 physical processes of ice slipping due to deformation of beds composed of water-saturated till. As detailed
 532 later in this section, natural glacier systems will, of course, be more complex than our model. Nevertheless,
 533 our model evinces rich dynamical behaviors consistent with observations, suggesting that our model strikes
 534 an appropriate balance between capturing the salient physical processes while remaining simple enough to
 535 allow for physical insight.

536 4.1 Mechanics of incipient surge motion

537 Rich dynamical behavior in our model is driven by the interactions of the three factors that define the shear
 538 strength of the till $\tau_t = (p_i - p_w)\mu$: the overburden pressure $p_i = \rho_i g h$, pore water pressure p_w , and
 539 the rate-and-state-dependent internal friction coefficient $\mu = \mu(u_b, \theta)$. To understand surge behavior in
 540 glaciers with till-covered beds, it is important to recognize that pore water pressure tends to decrease due to
 541 dilation, which strengthens till and resists surge motion, while the internal friction coefficient can increase
 542 or decrease, often by small amounts. Rate-weakening internal friction ($a - b < 0$) can help to facilitate
 543 surges but is not a necessary condition as surges are possible with rate-strengthening friction coefficients
 544 ($a - b > 0$) under conditions that allow for reduction in effective pressure (Fig. 5).

545 The key process governing incipient surge motion is suction caused by till dilation in relatively imper-
 546 meable till. In this case, pore water pressure decreases in response to shear-driven dilation, and the drop in
 547 pore water pressure diminishes the ability of till to evolve to a new steady state. If hydraulic permeability
 548 is sufficiently low (*i.e.*, if the diffusion time of the deforming till layer t_h is sufficiently long), slowing of
 549 state evolution allows the glacier to accelerate for longer periods of time. This longer acceleration phase

550 gives the glacier time to thin dynamically, which reduces the overburden pressure (p_i). In the region of the
 551 parameter space shown in Fig. 5, the reduction in overburden pressure outpaces drops in pore water pressure
 552 (p_w) leading to a net reduction in the effective pressure ($N = p_i - p_w$) and thereby the shear strength of till
 553 ($\tau_t = \mu N$). From Eqs. 24 and 32, we can see that the rate of change in driving stress is $\dot{\tau}_d \approx 2\dot{p}_i\alpha$, indicat-
 554 ing that driving stress evolves at least an order of magnitude more slowly than changes in overburden due
 555 to the shallow slopes of glaciers ($\alpha \ll 1$). As a result, reductions in overburden pressure facilitate sustained
 556 excess driving stress ($\tau_d > \tau_b$), the key ingredient for sustained incipient surge motion. It is necessary, then,
 557 that the initial acceleration must be large enough and last for long enough to generate sufficient dynamical
 558 thinning of the glacier.

559 4.2 Implications of surge mechanics

560 The need for dynamic thinning to sustain surge motion gives two necessary conditions for glacier surging:
 561 till must have sufficiently low hydraulic permeability to allow for incipient surge motion to be maintained
 562 over a long enough period of time, and the velocity during the nascent surge much exceed the balance
 563 velocity to allow for dynamical thinning. The latter condition implies a third necessary condition: shear
 564 strength of the till must be less than the balance driving stress, defined as the driving stress at which the
 565 balance velocity is achieved through internal deformation of the ice column. Consequently, yielding of the
 566 till must occur at glacier velocities slower than the balance velocity to allow for continual shear-loading of
 567 the till.

568 In the accumulation zones of surging glaciers, flow speeds must be slower than the balance velocity to
 569 build an ever-thickening reservoir of ice (Björnsson et al., 2003). This condition must persist throughout
 570 the quiescent phase because once the flow speed reaches the balance velocity, there would be no way to
 571 further increase driving stress and load the bed as ice-mass would be evacuated by flow accommodated
 572 through vertical shearing of the ice column. In other words, mass balance along with the geometric and
 573 rheological properties of surge-type glaciers allow them to build a reservoir that exerts a driving stress equal
 574 to bed failure strength before flow rates reach the balance velocity. To illustrate this point, consider that the
 575 maximum load a glacier can apply to its bed is given by the gravitational driving stress when the surface
 576 velocity of the ice equals the balance velocity and basal slip rate is negligible ($\tau_b \approx \tau_d$). Surface velocity
 577 due solely to vertical shearing within the ice column u_v is given by assuming that stress increases linearly
 578 with depth, that ice rheology is constant with depth, and that ice flow is parallel to the ice surface, yielding

$$u_v = \frac{2Ah\tau_d^n}{n+1}, \quad (33)$$

579 where A is the prefactor and n is the stress exponent in the constitutive relation for ice (Eq. 25). Defining
 580 the rate of change in driving stress as (cf. Eqs. 24, 31, and 32)

$$\dot{\tau}_d \approx 2\rho_i g \alpha^2 \zeta (u_* - u_s), \quad (34)$$

581 and setting $u_s = u_v = u_*$ in Eq. 34 gives the balance driving stress

$$\tau_{d*} = \tilde{\tau}_d \left(\frac{n+2}{2} \right)^{\frac{1}{n+1}} \approx 1.25 \tilde{\tau}_d, \quad (35)$$

582 where the potential drag at the bed is

$$\tilde{\tau}_d = \left(\frac{\rho_i g \dot{M}}{A} \right)^{\frac{1}{n+1}}, \quad (36)$$

583 whose variables \dot{M} , A , and, to a lesser extent, ρ_i are governed by local climate (Cuffey and Paterson,
 584 2010). Although mass density cannot vary more than 25%, \dot{M} and A can vary independently by orders of

585 magnitude. Thus, potential drag $\tilde{\tau}_d$ for an idealized glacier is determined almost exclusively by \dot{M}/A , the
 586 ratio of mass balance, \dot{M} , to the rate factor, A , which depends on ice temperature and interstitial meltwater
 587 content, along with crystallographic fabric (Minchew et al., 2018).

588 Eqs. 35 and 36 underpin a necessary condition for surging: At a minimum, surging glaciers must
 589 have a climate, and geometry, that allows for sufficiently high $\tilde{\tau}_d$ values—a combination of high mass
 590 balance and stiff ice (i.e. small A)—to overcome the strength of their beds. As a result, the geographic
 591 distribution of surge-type glaciers will reflect areas that combine sufficiently high rates of snowfall, relatively
 592 low summertime melt at the surface, and cold, stiff ice with beds that have yield stresses below the respective
 593 $\tilde{\tau}_d$ but are strong enough to allow the glacier to develop driving stresses that allow for order-of-magnitude
 594 increases in ice flow during the surge. Assuming that the pre-surge surface velocity, $u_{s_{pre}}$, in the region
 595 where a surge begins is primarily due to viscous deformation in the ice column (i.e., $\tau_{b_{pre}} \approx \tau_{d_{pre}}$) and
 596 considering that surface velocity at peak surge speeds, $u_{s_{surge}}$, is due primarily to basal slip, the gravitational
 597 driving stress necessary to produce a given speedup can be approximated as

$$\tau_{d_{pre}} \approx \tau_{t_{surge}} \left[1 - \frac{u_{s_{surge}} h_{surge}^n h_{pre}}{u_{s_{pre}} w^{n+1}} \right]^{-1/n}, \quad (37)$$

598 where $\tau_{t_{surge}}$ is the shear strength of the till when the glacier is flowing at peak surge speed. Note that
 599 typical values for the bracketed term in Eq. 37 will be approximately one for glaciers that are wider than
 600 they are thick (a condition stated at the beginning of the model derivation). Combining Eq. 37 with the
 601 balance velocity explicitly gives the necessary condition

$$\tau_{d_{pre}} < \tau_{d*}, \quad (38)$$

602 which to a good approximation is simply $\bar{\tau}_t < \tilde{\tau}_d$, where $\bar{\tau}_t$ is the long-term average shear strength of
 603 the till in the region where surges nucleate. The range of reasonable values on $\rho_i g$ is small, so to a good
 604 approximation, whether a glacier meets the condition in Eq. 38 is determined primarily by mass balance,
 605 ice rheology, bed strength, and cross-sectional aspect ratio (h/w).

606 The condition defined by Eqs. 35 through 38 yield surge conditions discussed in previous observa-
 607 tional studies. The dependence on mass balance is consistent with observations that have shown cumulative
 608 quiescent-phase mass balance to be a reliable predictor of surging on Variegated Glacier, Alaska (Eisen
 609 et al., 2001, 2005). The temperature-dependent ice rheology reproduces the climatic and geometric trends
 610 reported in (Sevestre and Benn, 2015) (Fig. 8). In this framework, warmer climate (and ice temperatures)
 611 require higher values of surface mass balance to satisfy the condition that the bed yields before the driving
 612 stress becomes high enough to cause the glacier to flow at the balance velocity through internal deformation
 613 within the ice.

614 Further insight into the spatial distribution and longer-term evolution of surge-type glaciers can be
 615 gleaned from the boundaries between surge-type and non-surge-type glaciers illuminated in the permeability
 616 vs evolution effect parameter space (Fig. 5). The sharp, diagonal boundary between surging on non-surge
 617 behavior suggests the existence of a Hopf bifurcation in the system and lies at values that are likely to be rel-
 618 atively rare in nature and closely linked to local lithology and degree of weathering. In particular, our model
 619 suggests that values of hydraulic diffusivity for till in surge-type glaciers falls in the lower range of observed
 620 values ($\sim 10^{-9}$ m²/s) for the range of b values explored in this study. Such low hydraulic diffusivities are
 621 consistent with canonical values of permeability expected for fine-grain sediments and loams (Lambe and
 622 Whitman, 1969; Cuffey and Paterson, 2010). The need for such low values of hydraulic permeability and
 623 fine-grained sediments suggests a potential role for comminution and sediment transport in activating and
 624 deactivating surging over millennial timescales, though future work is needed to elucidate these connections.

625 The governing role of till dilation and evolving pore water pressure in our model points to further meth-
 626 ods for testing the model in nature. In addition to the comparisons with data similar to those given in this

627 study (namely Fig. 7 and the preceding discussion of geographic distribution of surge-type glaciers), we
628 propose that passive seismic data collected during the incipient surge phase would provide valuable insight
629 into the salient processes and could be used to test our model. Passive seismic data are routinely used to
630 estimate the seismic moment from which estimates of the bulk shear modulus can be gleaned. The shear
631 modulus is sensitive to both the porosity and pore water pressure, and so can be used as a means to observe
632 till dilation and variations in pore water pressure.

633 4.3 Model limitations and future development

634 Our goal with this work is to better understand basal mechanics by developing a model for incipient surge
635 motion in glaciers with till-covered beds. We do not attempt to capture all of the processes that may be
636 important in initiating and sustaining glacier surges. As a result, our model has some limitations that provide
637 avenues for future work.

638 A notable limitation is the lack of explicit treatment for evolution of the subglacial hydrological system
639 during any stage of the surge or the quiescent phase. The influence of basal hydrological characteristics
640 is manifested in the model through the system water pressure p_{w_r} , but we implicitly treat this water pres-
641 sure as passive in the model development. A fully passive basal hydrological system is unlikely given the
642 rapid, extreme changes in glacier dynamics that define a surge. During surges, significant volumes of till
643 are displaced, filling most existing cavities, basal crevasses, or channels that constitute the contemporane-
644 ous hydrological system (Woodward et al., 2003). This lack of explicit treatment for changes in p_{w_r} due
645 to till displacement leaves open the possibility that increases in basal water pressure caused by changes in
646 the basal hydrological system can cause surges. What we have provided in this study are proposed mecha-
647 nisms of incipient surge motion in glaciers with deformable beds that are not dependent on changes in the
648 basal hydrological system. The existence of such a mechanism, which works equally well for temperate and
649 polythermal glaciers, and observations of surges beginning in times of the year when there is little or no ad-
650 ditional surface meltwater available to pressurize a basal hydrological system (e.g. during winter), supports
651 the hypothesis that it is the incipient surge motion that diminishes the efficiency of any extant hydrological
652 system rather than changes in the hydrological system that lead to surges.

653 We do not explicitly consider enhanced melting of basal ice through frictional heating or viscous dis-
654 sipation. The reason for this exclusion is twofold. First, melt-rates scale linearly with the product of basal
655 slip rate and till shear strength. While this product likely increases during the early surge phase, the trade-
656 off between diminished till shear strength, basal slip rate, and the characteristics of subglacial hydrological
657 systems is nontrivial and leads to melt rates that are orders of magnitude below surface meltwater fluxes in
658 many areas (Robel et al., 2013; Tulaczyk et al., 2000b). The second reason we exclude slip-induced melting
659 is that melting only influences ice dynamics through changes in basal and pore water pressure (Benn et al.,
660 2019). Without a reliable model for subglacial hydrology, there is no way to effectively link basal melt rate
661 and water pressure.

662 Our model does not capture the down-glacier propagation of mechanical, kinematic, or basal-water
663 pressure waves (Kamb et al., 1985; Fowler, 1987b). This limitation arises from the fact that our model is
664 essentially one-dimensional, meaning that we neglect extensional (along-flow normal) stresses and strain
665 rates (Eqs. 26 and 31) along with horizontal gradients in water pressure. During the quiescent phase,
666 neglecting extensional stresses is reasonable in the upper accumulation zone where surges are prone to
667 begin. Here, surface velocities tend to be slow and relatively consistent over large spatial scales, meaning
668 that along-flow strain rates are small relative to the effective strain rate; since ice is a viscous fluid, low strain
669 rates mean low stresses. During the surge, the surface velocities are high, with the exception of the period
670 when surge waves are present, and velocities can be expected to have small spatial gradients (Murray et al.,
671 2003; Dunse et al., 2015). A more complete model of glacier surges would include more terms of the stress
672 divergence such that it could account for the propagation of surge motion through the glacier. This more

673 complete model would be useful for further investigating the influence of glacier length on surge behavior
674 (Benn et al., 2019). However, we consider our box-model analysis to be a prerequisite to more complicated
675 flowline and 3D studies, which we reserve for future work.

676 **5 Summary and Conclusions**

677 In this paper, we develop a new model of incipient surge motion in glaciers with till covered beds. Incipient
678 surge motion in our model occurs in the absence of enhanced water flux to the bed, changes to the basal
679 hydrological system, and freeze-thaw cycles in till. Our model is based on granular mechanics of the till
680 and focuses on processes that can lead to unstable acceleration in glaciers with deformable beds. Our
681 model is unique among existing surge models in that it accounts for till porosity and pore water pressure,
682 and represents the evolution of internal friction, porosity, and pore water pressure within the deforming till
683 layer as a functions of the rate and history of shearing within the deforming till layer. This combination
684 of mechanisms allows for exploration of the rich dynamics that arise from changes in the three factors
685 that govern the shear strength of till: ice overburden pressure, pore water pressure, and the internal friction
686 coefficient. To represent these factors, we adopt the phenomenological rate-and-state model commonly used
687 in studies of slip on tectonic faults. We link the state variable, which encodes the history of basal slip, to till
688 porosity and derive a model in which pore water pressure evolves due to changes in porosity and transport
689 of pore water (*i.e.*, Darcy flow) into and out of the deforming till layer.

690 We find that till dilation, and more specifically suction caused by the reduction of pore water pressure
691 in response to dilation, is a fundamental control on incipient surge motion. This control arises from the
692 need for dynamic thinning of the glacier to sustain surge motion by reducing the effective pressure at the
693 bed. Glacier thinning is necessary because, following a perturbation, till tends toward a new steady state
694 while flow of water into and out of the deforming layer acts to equalize pore water pressure between the
695 underlying static till layer, the deforming till layer, and the subglacial hydrological system. As a result,
696 the shear strength of the bed tends to a new steady state, leading to stable acceleration, unless the glacier
697 thins. If the permeability of the till is sufficiently low, the evolution of the till to a new steady state is slow
698 enough to allow accelerated surge motion to thin the glacier, so long as flow speeds during the nascent surge
699 exceed the glacier’s balance velocity. Thinning of the glacier allows for unstable acceleration of the glacier
700 due to reductions in shear strength of the till, leading to order-of-magnitude increases in flow velocity that
701 characterize surges and are consistent with observations of glacier acceleration during surges.

702 The hydromechanical properties of till, namely the need for low till permeability, required to induce
703 rapid glacier thinning and surge motion give rise to restrictive conditions for glacier surges and rich dynam-
704 ics. The necessary conditions for surging illuminated by our model are low hydraulic permeability in the
705 deforming till layer, surge velocities that exceed the balance velocity, and maximum shear strength of till
706 that is less than the driving stress needed to achieve the balance velocity through vertical shearing in the ice
707 column. These conditions are consistent with the rarity of surge-type glaciers; the geographic and climatic
708 distribution and clustering of surge-type glaciers; and millennial-timescale evolution of surge behavior. Fur-
709 thermore, the rich dynamics produced by our model allow for abandoned surges along with a spectrum of
710 surge-like behaviors that are consistent with kinematic observations of natural glaciers but are lacking in
711 existing surge models.

712 Our model is necessarily simplified but contains important new physical processes — namely, till me-
713 chanics — that have been neglected in virtually all previous studies of glacier surges. To focus on the
714 complex processes of water saturated till, we deliberately ignore other processes that may be essential for a
715 complete understanding of surge dynamics. Most notably, we neglect extensional stresses and vertical shear-
716 ing in the ice column, and we treat the subglacial hydrological system as static. As a result, our model only
717 captures the incipient surge phase and not slowdowns that terminate surges. We derive our model such that
718 the inclusion of a dynamic subglacial hydrological system should be a relatively straightforward additions

719 and extension and vertical shear stresses can be included with the application of a more sophisticated flow
720 model that accounts for more terms of the stress divergence in the momentum equations. These avenues
721 provide numerous opportunities for future exploration of surge dynamics.

722 *Data access:* No new data are presented in this study. Source code for the numerical simulations is available
 723 at github.com/bminchew/glacier_surging1.git.

724 *Author contribution:* BM conceived the project, led the model development, and drafted the manuscript.
 725 CM provided essential insight, assisted with model development, and helped revise the manuscript.

726 *Competing Interests:* The authors declare no competing interests.

727 *Funding:* At various stages of this work, B.M. was partially funded by a NASA Cyospheric Sciences award
 728 NNX14AH80G, generous donations from the Albert Parvin and ARCS LA Chapter foundations, and an
 729 NSF Earth Science Postdoctoral Fellowship award EAR-1452587. C.M. acknowledges support from the
 730 David Crighton Fellowship, NSF-1144152 and NSF-1603907.

731 *Acknowledgements:* We thank James Rice, Alan Rempel, Bradley Lipovsky, Lucas Zoet, and Robert Viesca
 732 for insightful discussions.

733 **References**

734 M. F. Meier and A. Post. What are glacier surges? *Canadian Journal of Earth Sciences*, 6(4):807–817,
 735 1969.

736 C. Raymond. How do glaciers surge? A review. *Journal of Geophysical Research*, 92(B9):9121–9134,
 737 1987. doi: 10.1029/JB092iB09p09121.

738 B. Kamb. Glacier surge mechanisms based on linked cavity configuration of the basal water conduit system.
 739 *Journal of Geophysical Research*, 92(B9):9083–9100, 1987.

740 T. Murray, G. W. Stuart, P. J. Miller, J. Woodward, A. M. Smith, P. R. Porter, and H. Jiskoot. Glacier surge
 741 propagation by thermal evolution at the bed. *Journal of Geophysical Research: Solid Earth*, 105(B6):
 742 13491–13507, 2000. doi: 10.1029/2000JB900066.

743 A. C. Fowler, T. Murray, and F. S. L. Ng. Thermally controlled glacier surging. *Journal of Glaciology*, 47
 744 (159):527–538, 2001.

745 T. Murray, T. Strozzi, A. Luckman, H. Jiskoot, and P. Christakos. Is there a single surge mechanism?
 746 Contrasts in dynamics between glacier surges in Svalbard and other regions. *Journal of Geophysical*
 747 *Research*, 108(B5):1–15, 2003. doi: 10.1029/2002JB001906. 2237.

748 G. E. Flowers, N. Roux, S. Pimentel, and C. G. Schoof. Present dynamics and future prognosis of a slowly
 749 surging glacier. *The Cryosphere*, 5:299–313, 2011. doi: 10.5194/tc-5-299-2011.

750 C. R. Meyer, M. C. Fernandes, T. T. Creyts, and J. R. Rice. Effects of ice deformation on Røthlisberger
 751 channels and implications for transitions in subglacial hydrology. *Journal of Glaciology*, 62(234):750–
 752 762, 2016. doi: 10.1017/jog.2016.65.

753 G. E. Flowers, A. H. Jarosch, P. T. A. P. Belliveau, and L. A. Fuhrman. Short-term velocity variations
 754 and sliding sensitivity of a slowly surging glacier. *Annals of Glaciology*, 57(72):71–83, 2016. doi:
 755 10.1017/aog.2016.7.

756 D. I. Benn, A. C. Fowler, I. Hewitt, and H. Sevestre. A general theory of glacier surges. *Journal of*
 757 *Glaciology*, 65(253):701–716, 2019. doi: 10.1017/jog.2019.62.

758 H. Jiskoot, P. Boyle, and T. Murray. The incidence of glacier surging in Svalbard: evidence from multi-
 759 variate statistics. *Computational Geoscience*, 24(4):387–399, 1998.

- 760 H Sevestre and D I Benn. Climatic and geometric controls on the global distribution of surge-type glaciers:
761 implications for a unifying model of surging. *Journal of Glaciology*, 61(228):646–662, 2015.
- 762 H. Jiskoot, T. Murray, and P. Boyle. Controls on the distribution of surge-type glaciers in Svalbard. *Journal*
763 *of Glaciology*, 46(154):412–422, 2000.
- 764 M. Truffer, W. D. Harrison, and K. A. Echelmeyer. Glacier motion dominated by processes deep in under-
765 lying till. *Journal of Glaciology*, 46(153):213–221, 2000. doi: 10.3189/172756500781832909.
- 766 H. Björnsson, F. Pálsson, O. Sigurðsson, and G. Flowers. Surges of glaciers in Iceland. *Annals of Glaciology*,
767 36:82–90, 2003. doi: 10.3189/172756403781816365.
- 768 W. D. Harrison and A. S. Post. How much do we really know about glacier surging? *Annals of Glaciology*,
769 36:1–6, 2003.
- 770 J. Woodward, T. Murray, R. A. Clark, and G. W. Stuart. Glacier surge mechanisms inferred from
771 ground-penetrating radar: Kongsvegen, Svalbard. *Journal of Glaciology*, 49(167):473–480, 2003. doi:
772 10.3189/172756503781830458.
- 773 A. Fowler. *Mathematical Geoscience*. Springer, London, 2011.
- 774 B. Kamb, C. F. Raymond, W. D. Harrison, H. Engelhardt, K. A. Echelmeyer, N. Humphrey, M. M. Brugman,
775 and T. Pfeffer. Glacier surge mechanism: 1982–1983 surge of Variegated Glacier, Alaska. *Science*, 227
776 (4686):469–479, 1985. doi: 10.1126/science.227.4686.469.
- 777 H. Bjornsson. Hydrological characteristics of the drainage system beneath a surging glacier. *Nature*, 395
778 (6704):771–774, 1998. doi: 10.1038/27384.
- 779 Hamish Pritchard, Tavi Murray, Adrian Luckman, T Strozzi, and Stuart Barr. Glacier surge dynamics
780 of Sortebrae, east Greenland, from synthetic aperture radar feature tracking. *Journal of Geophysical*
781 *Research*, 110(F03005):1–13, 2005. doi: 10.1029/2004JF000233.
- 782 Douglas I. Benn, Lene Kristensen, and Jason D. Gulley. Surge propagation constrained by a persistent
783 subglacial conduit, Bakaninbreen-Paulabreen, Svalbard. *Annals of Glaciology*, 50(52):81–86, 2009. doi:
784 10.3189/172756409789624337.
- 785 V. Round, S. Leinss, M. Huss, C. Haemmig, and I. Hajsek. Surge dynamics and lake outbursts of Kyagar
786 Glacier, Karakoram. *The Cryosphere*, 11(2):723–739, 2017. doi: 10.5194/tc-11-723-2017.
- 787 K. Echelmeyer, R. Butterfield, and D. Cuillard. Some observations on a recent surge of Peters Glacier,
788 Alaska, U.S.A. *Journal of Glaciology*, 33(115):341–345, 1987.
- 789 J. J. Roush, C. G. Lingle, R. M. Guritz, D. R. Fatland, and V. A. Voronina. Surge-front propagation and
790 velocities during the early 1993–1995 surge of Bering Glacier, Alaska, U.S.A., from sequential SAR
791 imagery. *Annals of Glaciology*, 36:37–44, 2003.
- 792 A. Bevington and L. Copland. Characteristics of the last five surges of Lowell Glacier, Yukon, Canada, since
793 1948. *Journal of Glaciology*, 60(219):113–123, 2014. doi: 10.3189/2014JoG13J134.
- 794 T. Dunse, T. Schellenberger, J. O. Hagen, A. Käab, T. V. Schuler, and C. H. Reijmer. Glacier-surge mecha-
795 nisms promoted by a hydro-thermodynamic feedback to summer melt. *The Cryosphere*, 9:197–215, 2015.
796 doi: 10.5194/tc-9-197-2015.

- 797 G. de Q. Robin. Ice movement and temperature distribution in glaciers and ice sheets. *Journal of Glaciology*,
798 2(18):523–532, 1955.
- 799 D. R. MacAyeal. Binge/purge oscillations of the laurentide ice sheet as a cause of the north atlantic’s heinrich
800 events. *Paleoceanography*, 8(6):775–784, 1993. doi: 10.1029/93PA02200.
- 801 A. A. Robel, E. DeGiuli, C. Schoof, and E. Tziperman. Dynamics of ice stream temporal variability:
802 Modes, scales, and hysteresis. *Journal of Geophysical Research: Earth Surface*, 118(2):925–936, 2013.
803 doi: 10.1002/jgrf.20072.
- 804 C. R Meyer, A. A Robel, and A. W Rempel. Frozen fringe explains sediment freeze-on during heinrich
805 events. *Earth and Planetary Science Letters*, 524:115725, 2019. doi: 10.1016/j.epsl.2019.115725.
- 806 G. K. C. Clarke. Thermal regulation of glacier surging. *Journal of Glaciology*, 16(74):231–250, 1976.
- 807 G. K. C. Clarke, U. Nitsan, and W. S. B. Paterson. Strain heating and creep instability in glaciers and ice
808 sheets. *Reviews of Geophysics and Space Physics*, 15(2):235–247, 1977.
- 809 M. Sund, T. R. Lauknes, and T. Eiken. Surge dynamics in the Nathorstbreen glacier system, Svalbard. *The
810 Cryosphere*, 8:623–638, 2014. doi: 10.5194/tc-8-623-2014.
- 811 N. J. Wilson, G. E. Flowers, and L. Mingo. Mapping and interpretation of bed-reflection power from
812 a surge-type polythermal glacier, Yukon, Canada. *Annals of Glaciology*, 55(67):1–8, 2014. doi:
813 10.3189/2014AoG67A101.
- 814 K. Thøgersen, A. Gilbert, T. V. Schuler, and A. Malthe-Sørensen. Rate-and-state friction explains glacier
815 surge propagation. *Nature Communications*, 10(2823):1–8, 2019. doi: 10.1038/s41467-019-10506-4.
- 816 G. K. C. Clarke. Subglacial till: A physical framework for its properties and processes. *Journal of Geo-
817 physical Research: Solid Earth*, 92(B9):9023–9036, 1987. doi: 10.1029/JB092iB09p09023.
- 818 A. W. Rempel. A theory for ice-till interactions and sediment entrainment beneath glaciers. *Journal of
819 Geophysical Research*, 113:1–20, 2008. doi: 10.1029/2007JF000870. F01013.
- 820 L. K. Zoet, B. Carpenter, M. Scuderi, R. B. Alley, S. Anandkrishnan, C. Marone, and M. Jackson. The
821 effects of entrained debris on the basal sliding stability of a glacier. *Journal of Geophysical Research:
822 Earth Surface*, 118(2):656–666, 2013. doi: 10.1002/jgrf.20052.
- 823 C. R. Meyer, A. S. Downey, and A. W. Rempel. Freeze-on limits bed strength beneath sliding glaciers.
824 *Nature Communications*, 9(3242):1–6, 2018. doi: 10.1038/s41467-018-05716-1.
- 825 L. K. Zoet and N. R. Iverson. Rate-weakening drag during glacier sliding. *Journal of Geophysical Research:
826 Earth Surface*, 121(7):1206–1217, 2016. doi: 10.1002/2016JF003909.
- 827 Lucas K. Zoet and Neal R. Iverson. A healing mechanism for stick-slip of glaciers. *Geology*, 46(9):807–810,
828 2018. doi: 10.1130/G45099.1.
- 829 J. F. Thomason and N. R. Iverson. A laboratory study of particle ploughing and pore-pressure feedback:
830 a velocity-weakening mechanism for soft glacier beds. *Journal of Glaciology*, 54(184):169–181, 2008.
831 doi: 10.3189/002214308784409008.
- 832 N. R. Iverson, R. G. McCracken, L. K. Zoet, Í. Ö. Benediktsson, A. Schomacker, M. D. Johnson, and
833 J. Woodard. A theoretical model of drumlin formation based on observations at Múlajökull, Iceland. *Jour-
834 nal of Geophysical Research: Earth Surface*, 122(12):2302–2323, 2017. doi: 10.1002/2017JF004354.

- 835 R. O. Davis and A. P. S. Selvadurai. *Plasticity and Geomechanics*. Cambridge University Press, Cambridge,
836 England, first edition, 2002.
- 837 A. Fowler. On the rheology of till. *Annals of Glaciology*, 37:55–59, 2003. doi:
838 10.3189/172756403781815951.
- 839 M. Truffer, K. A. Echelmeyer, and W. D. Harrison. Implications of till deformation on glacier dynamics.
840 *Journal of Glaciology*, 47(156):123–134, 2001. doi: 10.3189/172756501781832449.
- 841 P. L. Moore and N. R. Iverson. Slow episodic shear of granular materials regulated by dilatant strengthening.
842 *Geology*, 30(9):843–846, 2002. doi: 10.1130/0091-7613(2002)030<0843:SESOGM>2.0.CO;2.
- 843 J. H. Dieterich. Modeling of rock friction. Part 1: Experimental results and constitutive equations. *Journal*
844 *of Geophysical Research*, 84(B5):2161–2168, 1979. doi: 10.1029/JB084iB05p02161.
- 845 A. Ruina. Slip instability and state variable friction laws. *Journal of Geophysical Research*, 88(B12):
846 10359–10370, 1983. doi: 10.1029/JB088iB12p10359.
- 847 B. Kamb. Rheological nonlinearity and flow instability in the deforming-bed mechanism of ice
848 stream motion. *Journal of Geophysical Research: Solid Earth*, 96(B10):16585–16595, 1991. doi:
849 10.1029/91JB00946.
- 850 B. D. Kilgore, J. H. Dieterich, and M. L. Blanpied. Velocity dependent friction of granite over a wide range
851 of conditions. *Geophysical Research Letters*, 20(10):903–906, 1993. doi: 10.1029/93GL00368.
- 852 N. R. Iverson, T. S. Hooyer, and R. W. Baker. Ring-shear studies of till deformation: Coulomb plastic
853 behavior and distributed strain in glacier beds. *Journal of Glaciology*, 44:634–642, 1998.
- 854 S. Tulaczyk, W. B. Kamb, and H. F. Engelhardt. Basal mechanics of Ice Stream B, west Antarctica:
855 1. Till mechanics. *Journal of Geophysical Research: Solid Earth*, 105(B1):463–481, 2000a. doi:
856 10.1029/1999JB900329.
- 857 R. LeB. Hooke. *Principles of Glacier Mechanics*. Cambridge University Press, New York, NY, second
858 edition, 2005.
- 859 N. R. Iverson. Shear resistance and continuity of subglacial till: hydrology rules. *Journal of Glaciology*, 56
860 (200):1104–1114, 2010. doi: 10.3189/002214311796406220.
- 861 N. R. Iverson and L. K. Zoet. Experiments on the dynamics and sedimentary products of glacier slip.
862 *Geomorphology*, 244:121–134, 2015. doi: 10.1016/j.geomorph.2015.03.027.
- 863 T. W. Lambe and R. V. Whitman. *Soil Mechanics*. Wiley, New York, NY, 1969.
- 864 S. Tulaczyk, W. B. Kamb, and H. F. Engelhardt. Basal mechanics of Ice Stream B, west Antarctica: 2.
865 Undrained plastic bed model. *Journal of Geophysical Research: Solid Earth*, 105(B1):483–494, 2000b.
866 doi: 10.1029/1999JB900328.
- 867 S. Fuller and T. Murray. Sedimentological investigations in the forefield of an Icelandic surge-type glacier:
868 implications for the surge mechanism. *Quaternary Science Reviews*, 21:1503–1520, 2002.
- 869 A A Robel, Christian G Schoof, and E Tziperman. Rapid grounding line migration induced by internal
870 ice stream variability. *Journal of Geophysical Research: Earth Surface*, 119(11):2430–2447, 2014. doi:
871 10.1002/2014JF003251.

- 872 A. A. Robel, C. Schoof, and E. Tziperman. Persistence and variability of ice-stream grounding lines on
873 retrograde bed slopes. *The Cryosphere*, 10(4):1883–1896, 2016. doi: 10.5194/tc-10-1883-2016.
- 874 C. Schoof. Ice-sheet accerleration driven by melt supply variability. *Nature*, 468(7325):803–806, 2010. doi:
875 10.1038/nature09618.
- 876 I. J. Hewitt. Seasonal changes in ice sheet motion due to melt water lubrication. *Earth and Planetary
877 Science Letters*, 371–372:16–25, 2013. doi: 10.1016/j.epsl.2013.04.022.
- 878 M. A. Werder, I. J. Hewitt, C. G. Schoof, and G. E. Flowers. Modeling channelized and distributed subglacial
879 drainage in two dimensions. *Journal of Geophysical Research: Earth Surface*, 118(4):2140–2158, 2013.
880 doi: 10.1002/jgrf.20146.
- 881 L. Lliboutry. General theory of subglacial cavitation and sliding of temperate glaciers. *Journal of Glaciol-
882 ogy*, 7(49):21–58, 1968.
- 883 B. Kamb. Sliding motion of glaciers: theory and observations. *Reviews of Geophysics*, 8(4):673–728, 1970.
- 884 A. C. Fowler. Sliding with cavity formation. *Journal of Glaciology*, 33:255–267, 1987a.
- 885 C. Schoof. The effect of cavitation on glacier sliding. *Proceeding of the Royal Society of London. Series A,
886 Mathematical and Physical Sciences*, 461:609–627, 2005. doi: 10.1098/rspa.2004.1350.
- 887 B. P. Lipovsky and E. M. Dunham. Slow-slip events on the Whillans Ice Plain, Antarctica, described using
888 rate-and-state friction as an ice stream sliding law. *Journal of Geophysical Research: Earth Surface*, 122
889 (4):973–1003, 2017. doi: 10.1002/2016JF004183. 2016JF004183.
- 890 C. McCarthy, H. Savage, and M. Nettles. Temperature dependence of ice-on-rock friction at realistic glacier
891 conditions. *Philosophical Transactions of the Royal Society A: Mathematical, Physical and Engineering
892 Sciences*, 375(2086):1–18, 2017. doi: 10.1098/rsta.2015.0348.
- 893 J. R. Rice. Constitutive relations for fault slip and earthquake instabilities. *Pure and Applied Geophysics
894 PAGEOPH*, 121(3):443–475, 1983.
- 895 P. Segall and J. R. Rice. Dilatancy, compaction, and slip instability of a fluid-infiltrated fault. *Journal of
896 Geophysical Research*, 100(B11):22155–22171, 1995. doi: 10.1029/95JB02403.
- 897 P. Segall and J. R. Rice. Does shear heating of pore fluid contribute to earthquake nucleation? *Journal of
898 Geophysical Research*, 111(B09316):1–17, 2006. doi: 10.1029/2005JB004129.
- 899 Jianye Chen, A R Niemeijer, and Christopher J Spiers. Microphysically Derived Expressions for Rate-
900 and-State Friction Parameters, a, b, and Dc. *Journal of Geophysical Research: Solid Earth*, 122(12):
901 9627–9657, 2017. doi: 10.1002/2017JB014226.
- 902 A. P. Rathbun, C. Marone, R. B. Alley, and S. Anandakrishnan. Laboratory study of the frictional rheology
903 of sheared till. *Journal of Geophysical Research*, 113(F2):1–14, 2008. doi: 10.1029/2007JF000815.
904 F02020.
- 905 P. Segall, A. M. Rubin, A. M. Bradley, and J. R. Rice. Dilatant strengthening as a mechanism for slow slip
906 events. *Journal of Geophysical Research*, 115(B12305):1–37, 2010. doi: 10.1029/2010JB007449.
- 907 J. H. Dieterich. Applications of rate- and state-dependent friction to models of fault slip and earthquake
908 occurrence. In G. Schubert, editor, *Treatise on Geophysics*, pages 107–129. Elsevier, Amsterdam, 2007.
909 doi: 10.1016/B978-044452748-6.00059-6.

- 910 A C Palmer and James R Rice. The Growth of Slip Surfaces in the Progressive Failure of Over-Consolidated
 911 Clay. *Proceedings of the Royal Society A: Mathematical, Physical and Engineering Sciences*, 332(1591):
 912 527–548, 1973. doi: 10.1098/rspa.1973.0040.
- 913 C. Marone and B. Kilgore. Scaling of the critical slip distance for seismic faulting with shear strain in fault
 914 zones. *Nature*, 362(618):618–621, 1993. doi: 10.1038/362618a0.
- 915 C. Marone, M. Cocco, E. Richardson, and E. Tinti. The critical slip distance for seismic and aseismic
 916 fault zones of finite width. In *Fault-Zone Properties and Earthquake Rupture Dynamics*, volume 94 of
 917 *International Geophysics*, pages 135–162. Academic Press, 2009. doi: 10.1016/S0074-6142(08)00006-5.
- 918 A. Damsgaard, D. L. Egholm, J. A. Piotrowski, S. Tulaczyk, N. K. Larsen, and C. F. Brødstrup. A new
 919 methodology to simulate subglacial deformation of water-saturated granular material. *The Cryosphere*, 9
 920 (6):2183–2200, 2015. doi: 10.5194/tc-9-2183-2015.
- 921 J.-P. Ampuero and A. M. Rubin. Earthquake nucleation on rate and state faults – aging and slip
 922 laws. *Journal of Geophysical Research: Solid Earth*, 113(B1):n/a–n/a, 2008. ISSN 2156-2202. doi:
 923 10.1029/2007JB005082. B01302.
- 924 J. H. Dieterich and B. D. Kilgore. Direct observations of frictional contacts: New insights for sliding
 925 memory effects. *Pure and Applied Geophysics*, 143:283–302, 1994.
- 926 J. H. Dieterich. Constitutive properties of faults with simulated gouge. In N. L. Carter, M. Friedman, J. M.
 927 Logan, and D. W. Stearns, editors, *Mechanical Behavior of Crustal Rocks: The Handin Volume*, pages
 928 103–120. American Geophysical Union, 1981. doi: 10.1029/GM024p0103.
- 929 J. R. Rice and A. L. Ruina. Stability of Steady Frictional Slipping. *Journal of Applied Mechanics*, 50(2):
 930 343–349, 06 1983. ISSN 0021-8936. doi: 10.1115/1.3167042.
- 931 Joseph Walder and Amos Nur. Porosity reduction and crustal pore pressure development. *Journal of Geo-*
 932 *physical Research: Solid Earth*, 89(B13):11539–11548, 1984. doi: 10.1029/JB089iB13p11539.
- 933 B. M. Minchew. *Mechanics of deformable glacier beds*. PhD thesis, California Institute of Technology,
 934 2016. Chapter 4, Appendix A.
- 935 Neal R Iverson, Robert W Baker, and Thomas S Hooyer. A ring-shear device for the study of till deforma-
 936 tion: Tests on tills with contrasting clay contents. *Quaternary Science Reviews*, 16(9):1057–1066, 1997.
 937 doi: 10.1016/S0277-3791(97)00036-X.
- 938 K. M. Cuffey and W. S. B. Paterson. *The Physics of Glaciers*. Elsevier, 4th edition, 2010.
- 939 G. S. Boulton and R. C. A. Hindmarsh. Sediment deformation beneath glaciers: Rheology and geo-
 940 logical consequences. *Journal of Geophysical Research: Solid Earth*, 92(B9):9059–9082, 1987. doi:
 941 10.1029/JB092iB09p09059.
- 942 G.S. Boulton, K.E. Dobbie, and S. Zatzepin. Sediment deformation beneath glaciers and its coupling to
 943 the subglacial hydraulic system. *Quaternary International*, 86(1):3–28, 2001. doi: doi:10.1016/S1040-
 944 6182(01)00048-9.
- 945 N. R. Iverson and R. M. Iverson. Distributed shear of subglacial till due to Coulomb slip. *Journal of*
 946 *Glaciology*, 47(158):481–488, 2001.
- 947 D. MacAyeal. Large-scale ice flow over a viscous basal sediment - Theory and application to Ice Stream-B,
 948 Antarctica. *Journal of Geophysical Research*, 94(B4):4071–4087, 1989.

- 949 B. M. Minchew, M. Simons, M. Morlighem, H. Björnsson, F. Pálsson, S. Hensley, and E. Larour. Plastic
950 bed beneath Hofsjökull Ice Cap, central Iceland, and the sensitivity of ice flow to surface meltwater flux.
951 *Journal of Glaciology*, 62(231):147–158, 2016. doi: 10.1017/jog.2016.26.
- 952 J. W. Glen. The creep of polycrystalline ice. *Proceedings of the Royal Society of London A*, 228(1175):
953 519–538, 1955.
- 954 Eric Jones, Travis Oliphant, Pearu Peterson, et al. SciPy: Open source scientific tools for Python, 2018.
955 version 1.1.0.
- 956 J. Mouginot, A. A. Björk, R. Millan, B. Scheuchl, and E. Rignot. Insights on the surge behavior of storstrøm-
957 men and l. bistrup bræ, northeast greenland, over the last century. *Geophysical Research Letters*, 45(11):
958 11,197–11,205, 2018. doi: 10.1029/2018GL079052.
- 959 B. M. Minchew, C. R. Meyer, A. A. Robel, G. H. Gudmundsson, and M. Simons. Processes controlling the
960 downstream evolution of ice rheology in glacier shear margins: Case study on Rutford Ice Stream, West
961 Antarctica. *Journal of Glaciology*, 64(246):583–594, 2018. doi: 10.1017/jog.2018.47.
- 962 O. Eisen, W. D. Harrison, and C. F. Raymond. The surges of Variegated Glacier, Alaska, USA, and their
963 connection of climate and mass balance. *Journal of Glaciology*, 47(158):351–358, 2001.
- 964 O. Eisen, W. D. Harrison, C. F. Raymond, K. A. Echelmeyer, G. A. Bender, and J. L. D. Gorda. Variegated
965 Glacier, Alaska, USA: a century of surges. *Journal of Glaciology*, 51(174):399–406, 2005.
- 966 A C Fowler. A theory of glacier surges. *Journal of Geophysical Research*, 92(B9):9111–9120, 1987b. doi:
967 10.1029/JB092iB09p09111.

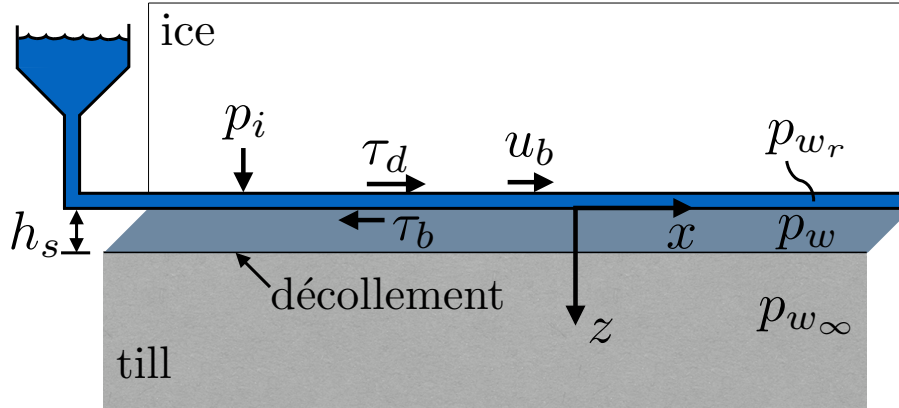


Figure 1: Model schematic showing a zoomed in view of the base of the idealized glacier with important parameters labeled.

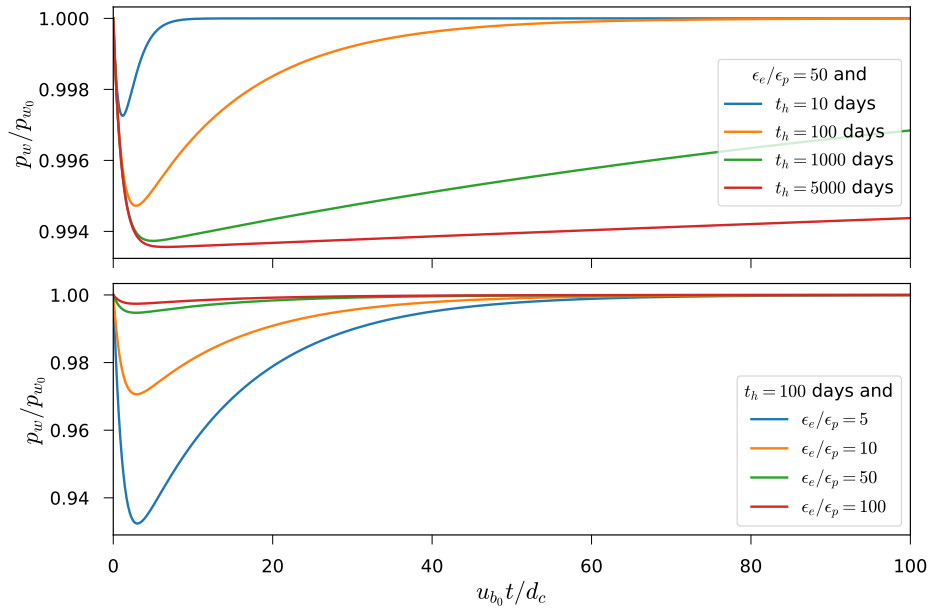


Figure 2: Evolution of pore water pressure in the deforming till layer (§33.1) following a step increase in basal slip rate, $u_b = 10u_{b_0}$ for $t \geq 0$, from an initial steady state ($\theta_0 = d_c/u_{b_0}$). The upper panel shows the influence of the hydraulic diffusion timescale of till on the evolution of pore water pressure for a fixed ϵ_e/ϵ_p ratio while the lower panel illustrates the influence of the ratio of the elastic to the plastic compressibility coefficients for a fixed diffusion timescale. Water pressures in the subglacial hydrological system (p_{w_r}) and underlying stagnant till layer (p_{w_∞}) are defined as $p_{w_r} = p_{w_\infty} = 0.9p_i$ and held constant in time. Other relevant parameters values are: $d_c = 0.1$, $\mu_n = 0.5$, $u_{b_0} = 10$ m/yr, $\phi_0 = 0.1$, and $p_{w_0} = p_{w_r} = p_{w_\infty}$.

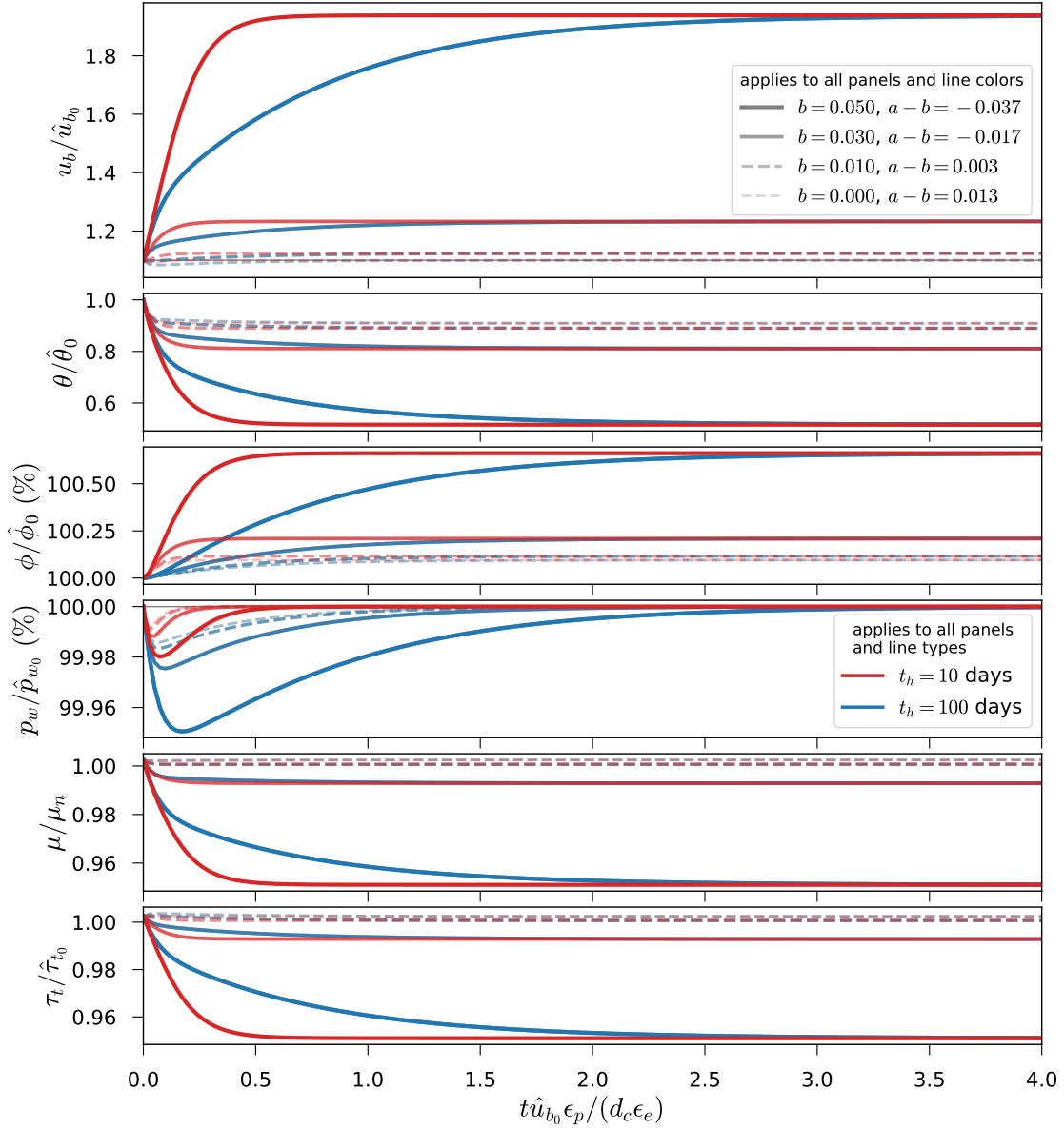


Figure 3: For fixed ice thickness §33.2: evolution of (from top to bottom) basal slip rate (u_b), state (θ), porosity (ϕ), pore water pressure in the deforming till layer (p_w), internal friction coefficient for till (μ), and till shear strength (τ_t) following a perturbation in basal slip rate from steady state. The perturbation in basal slip is $u_b = 1.1\hat{u}_b$ at $t = 0$, a value indicated by the thin solid gray line in the upper panel. We consider a range of evolution effects (b values, indicated by line widths and intensities in all panels) and two hydraulic diffusion timescales: $t_h = 10$ days (red lines in all panels) and $t_h = 100$ days (blue lines in all panels). In all panels, solid lines indicate rate-weakening ($a < b$) and dashed lines indicate rate-strengthening ($a > b$). Prescribed values are $\hat{u}_b = 10$ m/yr, $\hat{p}_w/p_i = 0.92$, $\hat{\phi}_0 = 0.1$, $d_c = 0.1$ m, $\epsilon_p = 10^{-3}$, $\epsilon_e = 50\epsilon_p$, $n = 3$, $\alpha = 0.05$, $a = 0.013$, and $\mu_n = 0.5$. Note that $d_c/\hat{u}_b = 0.01$ yr, making the total time on the horizontal axis 1 year. Here, we are interested in the response of the till only, so we hold glacier geometry constant.

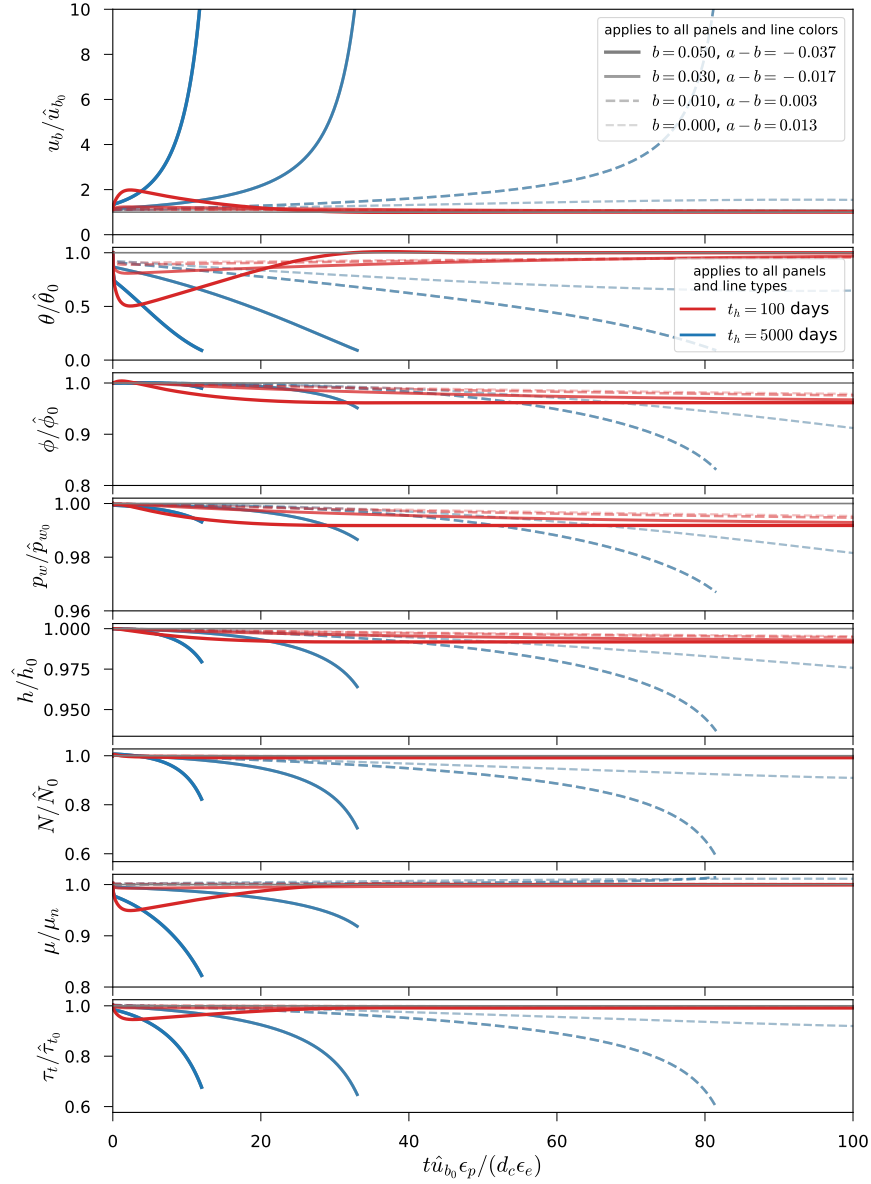


Figure 4: For variable ice thickness (§33.3): evolution of (from top to bottom) basal slip rate (u_b), state (θ), porosity (ϕ), pore water pressure in the deforming till layer (p_w), ice thickness (h), effective pressure (N), internal friction coefficient for till (μ), and till shear strength (τ_t) following a perturbation in basal slip rate from steady state. All factors are normalized by their respective initial steady state values. Velocity perturbation and other parameters are the same as for Fig. 3. Line thickness and continuity indicate different values of the evolution term b , as indicated in the legend in the upper panel, while line colors indicate values of the hydraulic diffusivity timescale for till (t_h), as shown in the legend in the third panel. Dashed lines indicate that the internal friction coefficient is rate-strengthening (*i.e.*, $(a - b) > 0$). Truncated lines occur when the integration is stopped; we chose $u_b/\hat{u}_{b_0} = 10$, which we define as indicating a surge, as the stopping condition. Over a long enough timescale, the line representing $b = 0$ and $t_h = 5000$ days eventually surges.

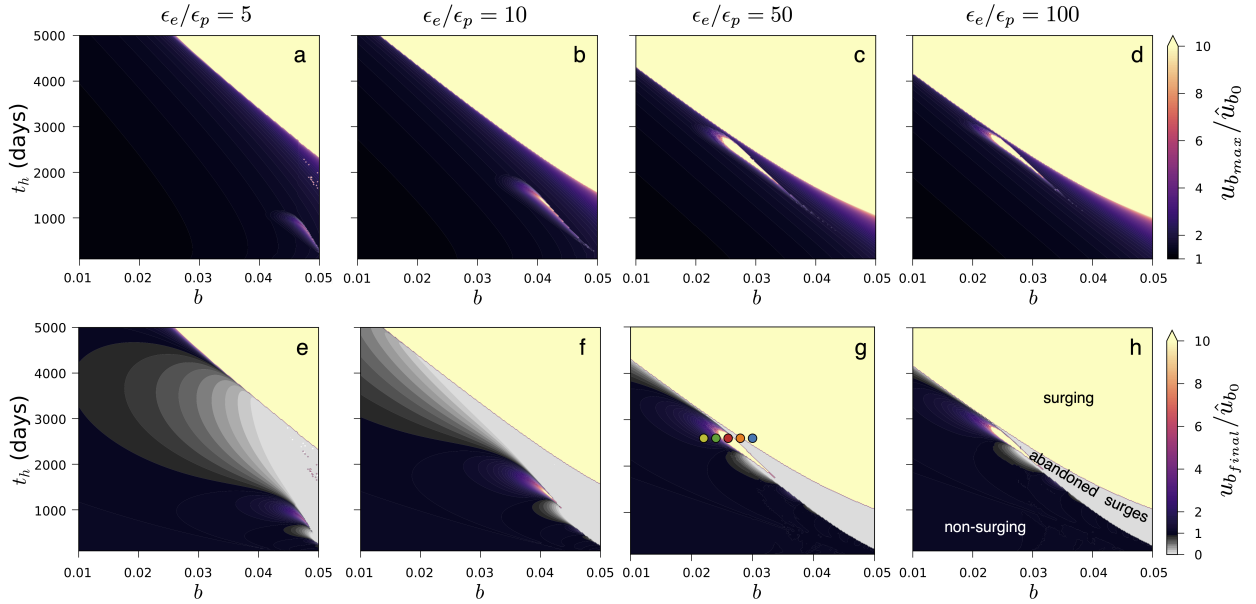


Figure 5: Parameter space covering the three principal parameters influencing incipient surge motion: the evolution effect b (x-axes of all panels), hydraulic diffusion timescale t_h (y-axes of all panels), and relative till compressibility ϵ_e/ϵ_p (columns). The top row (a–d) indicates the maximum basal slip rate ($u_{b_{max}}/\hat{u}_{b_0}$) achieved by the modeled glacier following a perturbation identical to that in Fig. 4, while the bottom row (e–h) shows the final basal slip rate ($u_{b_{final}}/\hat{u}_{b_0}$). Colored dots in (g) show the line colors and parameters for model outputs shown in Fig. 6. All other parameters are the same as in Fig. 4.

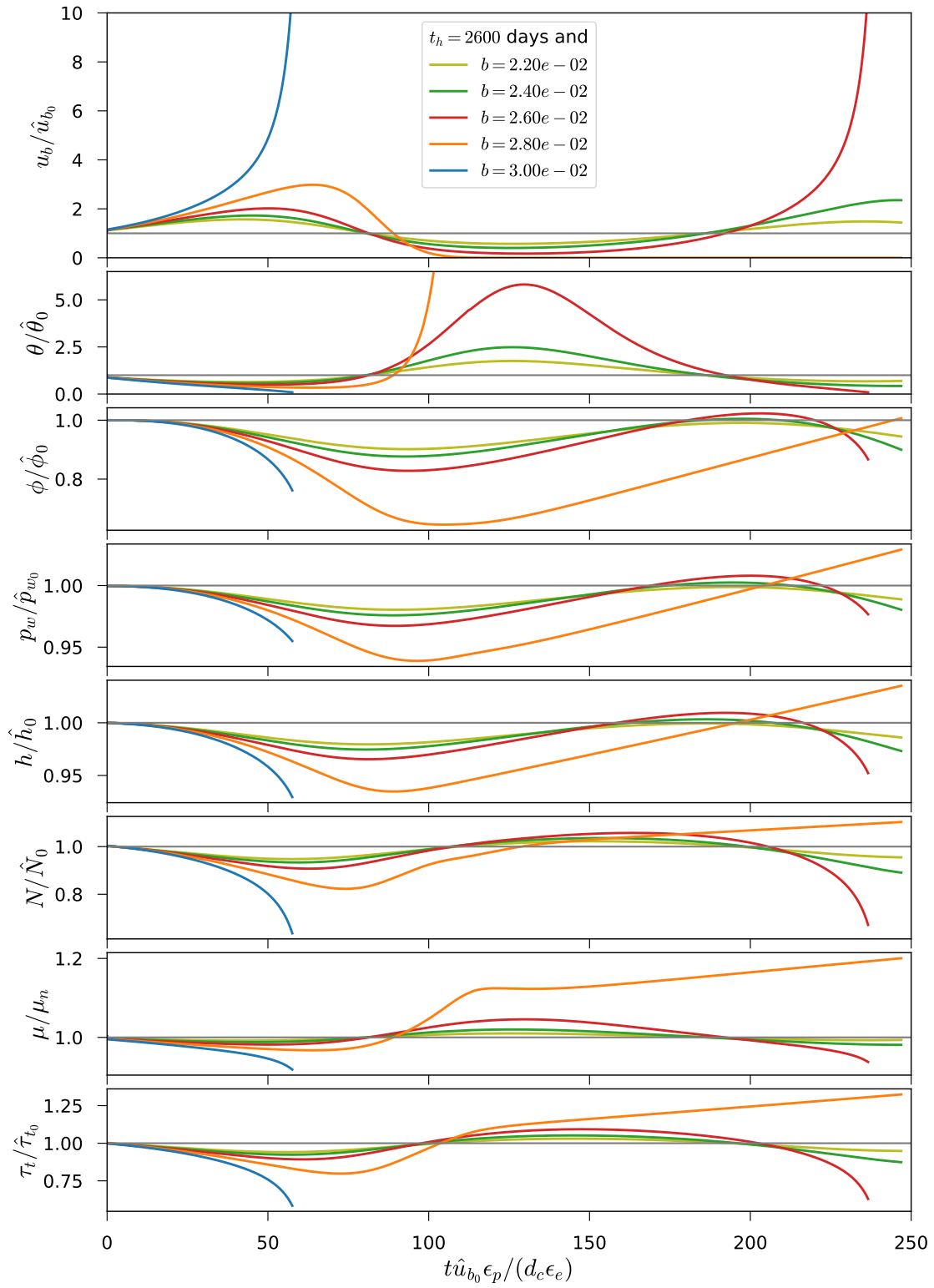


Figure 6: Similar to Fig. 4 except models are run using parameter values indicated in Fig. 5g. Line colors correspond to dot colors in Fig. 5g.

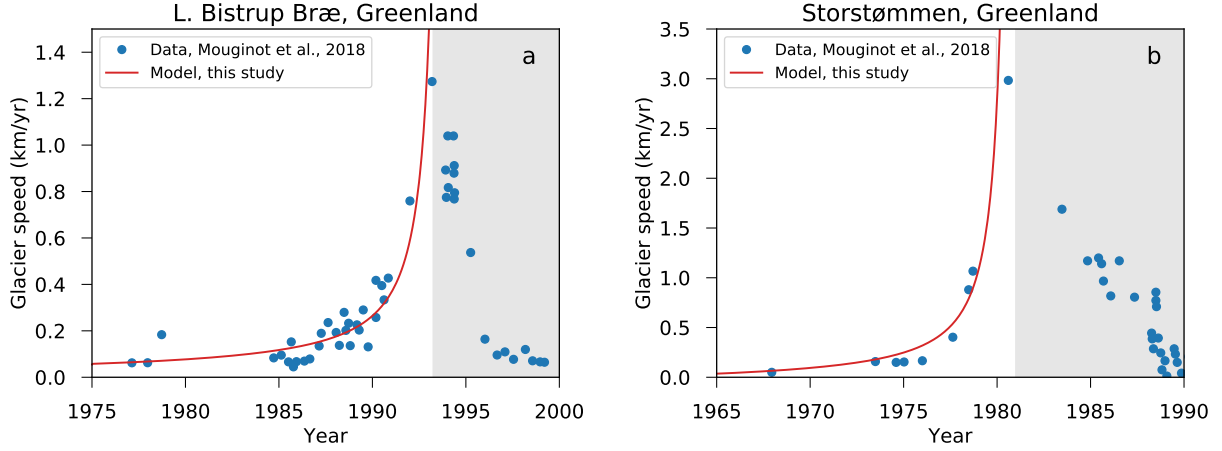


Figure 7: Comparison between our model and observed glacier surface velocities from two surges, (a) L. Bistrup Bræ and (b) Storstømmen, northeast Greenland (Mouginot et al., 2018). Model parameters are the same as in Fig. 3 and 4, and with $b = 0.03$, $t_h = 3000$ days, and initial velocity set according to the data. The grayed regions indicate the slowdown phase of the surge, which our model does not attempt to represent.

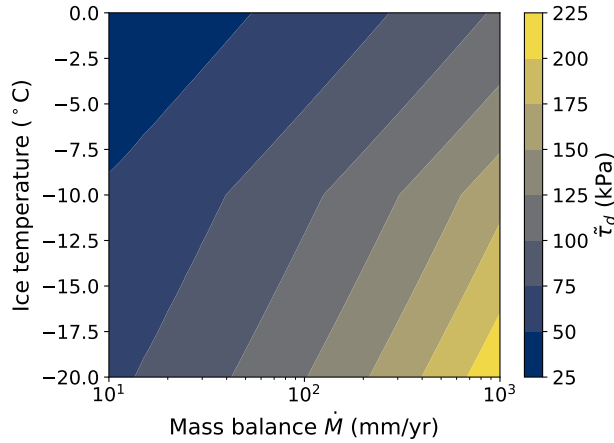


Figure 8: Potential drag at the bed $\tilde{\tau}_d$ (Eq. 36) as a function of surface mass balance (\dot{M}) and ice temperature. The rate factor is taken to depend on ice temperature T according to the Arrhenius relation $A = A_* \exp \{-Q_c (T^{-1} - T_*^{-1}) / R\}$, where $T_* = -10$ °C, $A_* = 3.5 \times 10^{-25}$ Pa $^{-3}$ s $^{-1}$, Q_c is the activation energy that increases from 60 kJ/mol for $T \leq T_*$ to 115 kJ/mol for $T_* < T \leq 0$ °C, and $R = 8.314$ J/(K·mol) is the ideal gas constant (Cuffey and Paterson, 2010).